therapy, retroviral vectors expressing herpes simplex virus-thymidine kinase (HSV-*tk*) combined with treatment with the prodrug ganciclovir (GCV) have been developed [1]. However, this system still has two hurdles, namely, the transduction efficiency of tumors and immune responses generated against the vectors [2]. In addition, it is essential that the vector has a tumor tracking property to effectively attack invasive or metastatic lesions with minimal adverse effects [3].

Mesenchymal stem cells (MSCs), as derived from adult bone marrow, fat, or fetal tissues, are a promising tool for regenerative medicine because of their self-renewal capacity and multilineage differentiation ability. Recent evidence suggests that bone marrow-derived MSCs selectively accumulate at tumors, and they are promising vehicles for tumor-targeting therapy [4,5]. However, MSCs may provide structural support to malignant cells and locally attenuate the tumor surveillance system through their immunosuppressive effects, leading to the progression of tumor growth [6–8]. Therefore, MSCs should be modified to have an increased antitumor activity in order to use them for cancer gene therapy [5,9,10].

Systemic administration of genetically modified MSCs to produce an anticancer cytokine has been shown to be effective in tumor suppression. Intravenous injection of MSCs expressing interferon (IFN)-β inhibits the expansion of the pulmonary metastasis of melanoma and breast cancer in mice [11] and prolongs the survival of mice with glioma xenografts [4]. For more efficient and specific MSC-based gene therapy, we aimed to develop MSCs with a vector-producing property.

In the present study, we developed MSCs that locally produce the HSV-*tk*-expressing retroviral vectors (VP-MSCs), which facilitate transgene transduction and tumor targeting. By using a mouse subcutaneous glioma model, we examined tumor tropisms and cancer-killing effects of systemically administered VP-MSCs. To assess the safety of this system, we demonstrated that tumor-specific transduction was achieved by the progeny retroviruses produced by VP-MSCs at the site of tumors.

Materials and methods

Cell culture

The malignant rat glioma cell line 9L and fibroblasts derived from a normal rat Rat-1 were obtained from the Riken BRC Cell Bank (Ibaraki, Japan) [12]. The stable firefly luciferase-expressing rat MSCs and 9L (9L/LNCL) were developed by transduction with a recombinant retroviral vector encoding luciferase and neomycin resistance genes. The cells were cultured in Dulbecco's modified Eagle's medium and nutrient mixture F12 (DMEM-F12; Invitrogen, Grand Island, NY, USA) and 10% fetal bovine serum (FBS; Sigma Chemical Co., St Louis, MO, USA) supplemented with 100 units/ml of penicillin and 100 μg/ml of streptomycin in an atmosphere of 5% CO_2 at 37 °C.

MSC isolation and culture

All animal experiments were approved by the Jichi Medical University ethics committee and were performed in accordance with the National Institutes of Health Guide for the Care and Use of Laboratory Animals. MSCs were prepared from the rat bone marrow as described previously [13]. Briefly, 5-week-old male Sprague-Dawley (SD) rats (Clea Japan, Tokyo, Japan) were sacrificed by an overdose of isoflurane inhalation, and their femurs and tibias were dissected. After the epiphyses were removed, the bone marrow was flushed out with DMEM-F12. A single cell suspension was obtained by sequential drawing of the marrow into syringes through 27-G needles. The cells were cultured at a density of 1×10^6 cells/cm^2 in noncoated T-25 or T-75 cell culture flasks containing DMEM-F12 and 10% FBS supplemented with 100 units/ml of penicillin and 100 μg/ml of streptomycin in an atmosphere of 5% CO_2 at 37 °C. After 3 or 4 days of culture, the medium was replaced and the non-adherent cells removed. Thereafter, the medium was then changed twice weekly. When 60–80% confluence was attained, the adherent cells were placed at a density of 1×10^4 cells/cm^2 in a T-225 flask for expansion. After 15 passages, the cells were used for the experiments.

VP- and non-VP-MSC preparation

HSV-*tk* or the firefly luciferase expression cassette was cloned into pLTR to create pLTR-*tk* or pLTR-*luc*. pGP and pVSV-G express the Moloney murine leukemia virus gag-pol and the vesicular stomatitis virus-G (VSV-G) pseudotyped envelope protein under the control of a cytomegalovirus promoter, respectively [12]. Nucleofection of MSCs was performed according to the manufacturer's instructions (Amaxa Biosystem, Cologne, Germany). To generate VP-MSCs, 2×10^6 MSCs were gently resuspended in 100 μl of Human Mesenchymal Nucleofector Solution (Amaxa Biosystem) and mixed with the proviral plasmids pGP, pVSV-G and pLTR-*tk* or pLTR-*luc* at concentrations of 1, 1 and 2 μg, respectively. The mixture was then pulsed with the program U-23. Non-VP-MSCs were generated by nucleofection with pLTR-*tk* or pLTR-*luc* alone. Vector-producing HEK293 (VP-293) cells and non-VP-293 cells were similarly developed by nucleofection using the X-01 pulse program. Cells were cultured in six-well plates containing prewarmed DMEM-F12 before the experiments. Quantification of RNA genome titer in culture supernatant was determined by reverse transcription-quantitative polymerase chain reaction (PCR) using a Retrovirus Titer Set (Takara Bio Inc., Shiga, Japan) according to the manufacturer's instructions. The results of viral titer were expressed as genomes/μl.

DOI: 10.1002/jgm

Transduction of 9L cells and MSCs with progeny retrovirus produced by VP-MSCs

The 100-μl culture supernatants of luciferase-expressing VP-MSCs or non-VP-MSCs in a 96-well plate after 24 h of nucleofection were added to 9L cells or MSCs (1×10^4 cells for each well) in a 96-well plate. After 48 h of incubation, transduction efficiency was estimated by the luciferase assay using a chemiluminometer (Fluoroskan Ascent FL, Thermo Labsystem, Beverly, MA, USA) and the Bright-Glo Reagent kit (Promega, Madison, WI, USA) according to the manufacturer's instructions.

Chemiluminescence assay for evaluating tumor-killing effects *in vitro*

9L/LNCL cells stably expressing luciferase were used in the present study. Briefly, 5×10^4 9L/LNCL cells were cocultured with 2.5×10^4 VP-MSCs or non-VP-MSCs in 48-well flat-bottomed plates (day 0). At day 3, the cells were exposed to varying concentrations (0.01–100 μmol/l) of GCV (F. Hoffmann-La Roche, Basel, Switzerland). At day 7, the luciferase assay was performed with a chemiluminometer (Thermo Labsystem) using the Bright-Glo Reagent kit (Promega) according to the manufacturer's instructions.

Determination of HSV-tk transgene copy number *in vitro*

To estimate the copy number of transgene in the cells transduced with retroviral progeny, 9L cells and MSCs were co-cultured and whole cells were collected at day 7. Quantitative values were obtained from the threshold cycle (Ct) number that indicated exponential amplification of the PCR product by using a sequence detection system (ABI Prism 7700; Applied Biosystems, Madison, WI, USA). The relative copy number of the HSV-*tk* gene was determined as the ratio of the copy numbers in the group of 9L cells co-cultured with VP-MSCs to the copy numbers in the non-VP-MSC group. The copy number of the reference gene *GAPDH* was also determined to correct the variation in the DNA amount and amplification efficiency. The gene specific primers are shown below: HSV-*tk* forward, 5′-CGTCGCCGATGGGGTGTTCT-3′, reverse, 5′-GCGCGGCCGGGTAGCACAGG-3′, rat *GAPDH* forward, 5′-CAGCAATGCATCCTGCAC-3′, and reverse, 5′-GAGTTGC-TGTTGAAGTCACAGG-3′.

In vivo bioluminescence imaging for detecting transgene expression

9L cells or Rat-1 cells (3×10^6 each) in 100 μl of phosphate buffer saline (PBS) containing 25% (v/v) basement membrane matrix (Matrigel; BD Biosciences, Franklin Lakes, NJ, USA) were subcutaneously inoculated into the bilateral dorsal region (3×10^6 cells/site) of 4- to 6-week-old male Balb/c nu/nu mice (Clea Japan). Immediately after inoculation, the luciferase-expressing VP-MSCs or non-VP-MSCs (5×10^5 cells/body each) were injected into the left ventricular cavity of mice. Three experimental groups were formed: group 1, mice inoculated with Rat-1 cells and injected with non-VP-MSCs; group 2, mice inoculated with 9L cells and injected with non-VP-MSCs; and group 3, mice inoculated with 9L cells and injected with VP-MSCs; $n = 4$ for each group. After injection of the cells, optical bioluminescence imaging was performed to periodically trace the cells using an *in vivo* imaging system (IVIS; Xenogen, Hopkinton, MA, USA). The reporter substrate D-luciferin (75 mg/kg body weight) was injected into the mouse peritoneum for scanning. The luminescence levels in the region of interest (total flux; photons/sec) were analysed using the Living Image software (Xenogen, Alameda, CA, USA).

Immunohistochemistry

Mice were anesthetized with an overdose of isoflurane inhalation and fixed by perfusion with 4% paraformaldehyde. The tissues were then embedded in an optimal cutting temperature compound (Sakura Finetek, Tokyo, Japan), frozen, and sectioned into 20-μm-thick slices. Immunohistochemical staining was performed with a rabbit monoclonal anti-luciferase antibody (1 : 5000; Promega) by the avidin-biotin-peroxidase method. Irrelevant rabbit immunoglobulin (Ig)G (Promega) was used as a negative control. Sections were treated with horseradish peroxidase-labelled anti-rabbit IgG secondary antibody (Dako, Glostrup, Denmark; 1 : 200), and luciferase-positive cells were visualized using the Vectastain Elite ABC kit (Vector Laboratories, Burlingame, CA, USA). The sections were counterstained with hematoxylin.

Determination of luciferase transgene copy number *in vivo*

To estimate the copy number of transgene in tissues in tumor-bearing mice, small pieces of tissues were obtained from peripheral and central portions of the tumors at 21 days after MSC administration. Quantitative values were obtained from the threshold cycle (Ct) number that indicated exponential amplification of the PCR product by using the sequence detection system (ABI Prism 7700). The relative copy number of the *luciferase* gene was determined as the ratio of the copy numbers in the peripheral or central portions of tumors in the group of 9L tumor in mice inoculated with VP-MSCs to the copy numbers in non-VP-MSCs group. The copy number of the reference gene *GAPDH* was also determined to correct for variation in the DNA amount

DOI: 10.1002/jgm

and amplification efficiency. The gene specific primers were: *Luc* forward, 5′-TTCTGGGGGCGCACCTCTTC-3′, and reverse, 5′-GGGGGCCACCTGATATCCTTTGTA-3′.

Survival of MSCs at the tumor sites *in vivo*

The stable luciferase-expressing MSCs were mixed with an equal number of nontransduced 9L cells (1.5×10^6 cells each) and were suspended in 100 μl of PBS containing 25% (v/v) Matrigel. Immediately, the mixture was subcutaneously inoculated into the bilateral dorsal region of nu/nu mice ($n = 4$ for each group). Luminescence at the tumor sites was periodically determined using IVIS (Xenogen), and the luminescence levels were analysed using Living Image software (Xenogen).

Assessment of tumor-specific transduction

To estimate the level of progeny retroviral transduction, PCR analysis was performed. DNA was extracted from the tumors or normal tissues by using a DNA extraction kit (Qiagen) at 21 days after MSC injection and then amplified using Ex Taq (Takara Bio Inc.). The PCR products (560 bp) extending from the 5′ long-terminal repeat (LTR) or 3′-LTR of the retroviral vector were produced using the gene-specific primers: LTR forward, 5′-AGGGCCAAGAACAGATGAGACAGC-3′ and reverse, 5′-GTACAGACGCAGGCGCATAACATC-3′. Conversion of the 3′-LTR to the 5′-LTR after retroviral transduction was confirmed by the typical banding pattern (440 bp + 120 bp fragments) generated after *Xba*I digestion.

Assessment of the anticancer effects of VP-MSCs *in vivo*

9L/LNCL cells (3×10^6 each) in 100 μl of PBS containing 25% (v/v) Matrigel were subcutaneously inoculated in the bilateral dorsal region of 4- to 6-week-old male Balb/c nu/nu mice. PBS (group 1), MSCs (group 2), HSV-tk-expressing non-VP-MSCs (group 3) or VP-MSCs (group 4; 5×10^5 cells/body each) were then injected into the left ventricular cavity of the mice ($n = 4$ for each group). Seven days after MSC injection, GCV (100 mg/kg/day) or PBS was continuously administered into the peritoneum by using mini-osmotic pumps (Alzet, Palo Alto, CA, USA) for 28 days. The tumor growth was monitored two or three times a week by measuring tumor sizes using a caliper, and tumor volumes were calculated using the formula: tumor volume (mm^3) = $a(mm) \times b^2(mm^2) \times 0.5$ (a, the height of the tumor; b, the width of the tumor).

Statistical analysis

Data from multiple experiments are expressed as the mean ± SEM. Statistical analyses were performed using StatView (Abacus Concepts, Inc., London, UK). Differences in parameters were evaluated by analysis of variance combined with Welch's t-test. $p < 0.05$ was considered statistically significant.

Results

Characterization of VP-MSCs

Consistent with previous studies, the bone marrow-derived rat MSCs used in the present study exhibited a spindle shape; they differentiated into adipocytes, osteocytes, and chondrocytes in appropriate culture media (data not shown). The green fluorescence protein (GFP)-based semiquantitative analysis revealed that nucleofection is more efficient for the transfection of MSCs than the calcium-phosphate method and lipofection: the percentage of GFP-positive MSCs after 24 h of transfection by each method was approximately 60.1%, 3.1% and 12.3%, respectively.

The secretion of retroviral vectors into the culture media of VP-MSCs (Figure 1a) and VP-293 cells (Figure 1b) increased and peaked at 48 h after nucleofection, whereas the vector production from non-VP-MSCs or non-VP-293 cells was undetectable. There was no significant difference in the amounts of produced vectors at 48 h between VP-MSCs and VP-293 cells.

Chemiluminescence assay showed that 9L glioma cells were efficiently transduced with the vectors generated from VP-MSCs (Figure 1c). On the other hand, when MSCs were treated with the culture media of VP-MSCs or non-VP-MSCs, transduction was undetectable (Figure 1d).

Tumor-killing effects of VP-MSCs *in vitro*

The *in vitro* luciferase assay revealed that the bioluminescence signal of luciferase-expressing 9L/LNCL cells decreased in a GCV dose-dependent manner after coculture with HSV-*tk*-expressing MSCs (Figure 1e). The concentration required to induce a 50% inhibition (IC_{50}) value of GCV in the presence of VP-MSCs at day 7 was considerably lower than that in the presence of non-VP-MSCs (0.33μmol/l versus 83μmol/l). At this time-point, real-time PCR analysis showed that the relative copy number of the HSV-*tk* gene in the VP-MSC group was approximately 17.5-fold more than that in the non-VP-MSC group (Table 1). Because transduction of MSCs with progeny retrovirus was inefficient (Figure 1d), these data suggests that 9L glioma cells were mainly transduced with progeny luciferase-expressing retrovirus produced by VP-MSCs (Figure 1c).

DOI: 10.1002/jgm

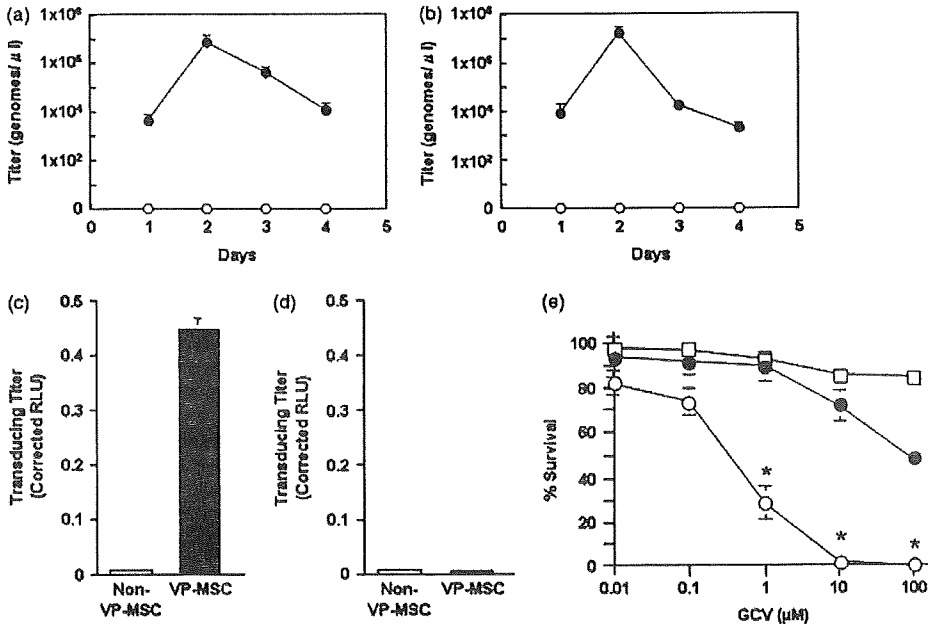

Figure 1. Function of vector-producing mesenchymal stem cells (VP-MSCs) *in vitro*. (a, b) Time course of luciferase-expressing retrovirus production from VP-MSCs and vector-producing HEK293 (VP-293) cells. VP-MSCs (a, ●; $n = 3$) or VP-293 (b, ●; $n = 3$) were developed with pGP, pVSV-G, and pLTR-*luc* at concentrations of 1, 1 and 2 μg by nucleofection. Non-VP-MSCs (a, ○; $n = 3$) or non-VP-293 (b, ○; $n = 3$) were developed with pLTR-*luc* by nucleofection. The RNA genome titer of progeny virus in the culture supernatant of these cells was determined by reverse transcription-quantitative PCR. (c, d) Transduction of rat glioma 9L cells (c) or MSCs (d) with luciferase-expressing retrovirus produced by VP-MSCs. The 9L cells and MSCs were treated with the culture supernatant of non-VP-MSCs (open bar; $n = 3$) or VP-MSCs (solid bar; $n = 3$) that were nucleofected 2 days before. The luminescence levels of these cells were measured by a chemiluminescence luciferase assay after 48 h of treatment. (e) Tumor-killing effects of VP-MSCs *in vitro*. MSCs were cocultured with luciferase-expressing 9L/LNCL glioma cells at a ratio of 1 : 3 (day 0), and different doses of GCV (0.01–100 mmol/l) were added to the culture media on day 3. The number of viable 9L/LNCL cells was estimated by a luciferase assay on day 7. The groups were as follows: MSCs without genetic modification (□); MSCs nucleofected with herpes simplex virus-thymidine kinase (HSV-*tk*)-expressing plasmid (non-VP-MSCs, ●); and MSCs nucleofected with retroviral vector components pLTR-*tk*, pGag-pol, and pVSV-G (VP-MSCs, ○). For each group, $n = 3$; $^*p < 0.05$ versus non-VP-MSC group

Table 1. Relative HSV-*tk* transgene copy number in the co-cultures of 9L tumor cells and MSCs

	Relative HSV-*tk* transgene copy number
Non-VP-MSCs	1.0
VP-MSCs	17.5

9L cells and MSCs were co-cultured and whole cells were collected at day 7. The relative copy number of the HSV-*tk* gene was determined as the ratio of the copy numbers in the group of 9L cells co-cultured with VP-MSCs to the copy numbers in the non-VP-MSC group. The copy number of the reference gene *GAPDH* was also determined to correct the variation in the DNA amount and amplification efficiency.

Tumor tropism of VP-MSCs *in vivo* and enhanced transgene expression *in situ*

In vivo imaging indicated that luciferase-expressing MSCs transiently appeared just after injection at high perfusion organs, such as the brain, liver, kidney and spleen, irrespective of administration of VP- or non-VP-MSCs (day 0). After systemic administration of non-VP-MSC, the signal peaked at day 10 and declined thereafter at the tumor sites, whereas no signal enhancement was observed at the site of Rat-1 inoculation (Figures 2a and 2b). By contrast, the signal after administration of VP-MSCs further increased over day 21 (Figures 2c and 2d), and no signal was observed in the normal organs at this time-point. Immunohistochemical studies showed marked luciferase expression at the tumor periphery in the VP-MSC group after 21 days of administration (Figure 2e). No signal of luciferase expression was observed in the normal tissues at this time-point. Real-time PCR analysis revealed that the relative copy number of the luciferase gene at the tumor periphery of the VP-MSC group was approximately 47.5-fold more than that of the non-VP-MSC group (Table 2). These results indicate not only successful retroviral vector production by VP-MSCs, but also effective gene transfer by progeny retrovirus *in situ*.

Survival of MSCs at the tumor site

The enhanced signal observed in the VP-MSC group may be in part due to expansion or division of VP-MSCs *in situ*. To exclude this possibility, we estimated the survival of MSCs in the vicinity of the 9L tumor. We employed stable luciferase-expressing MSCs to avoid the conditions of transient gene expression. When the cells were inoculated with 9L tumor cells at the dorsal region

DOI: 10.1002/jgm

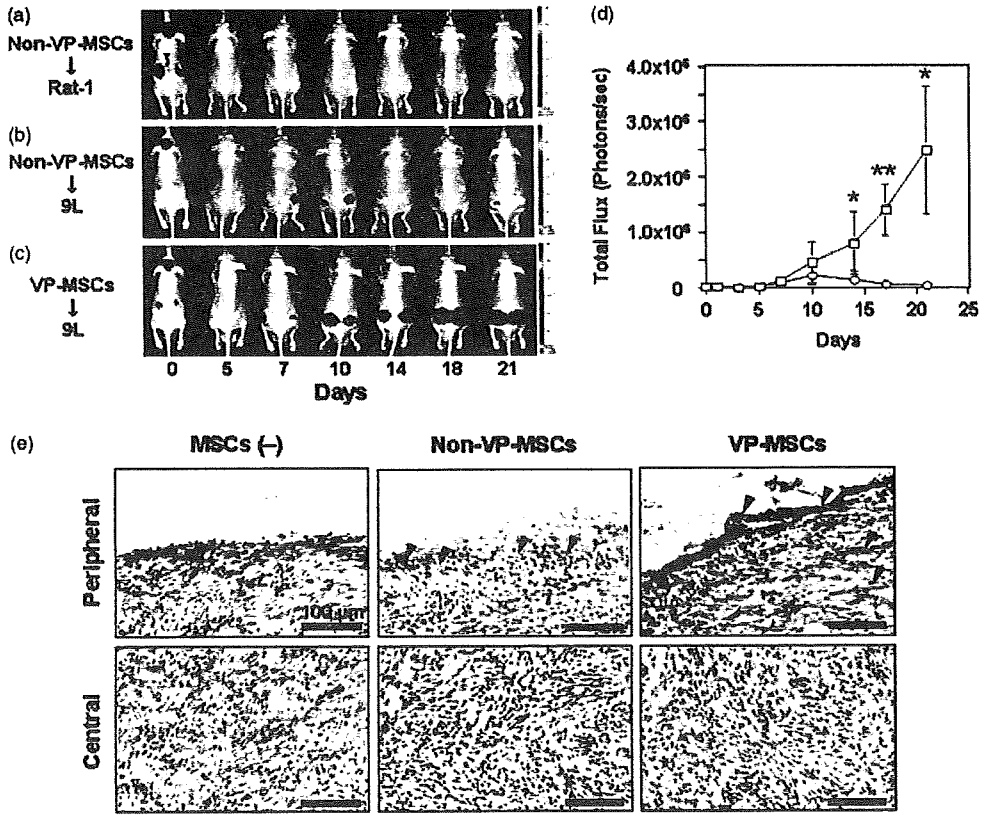

Figure 2. Tumor tropism and enhanced transgene expression after VP-MSC administration. Rat-1 fibroblasts (a) or 9L glioma cells (b, c) were subcutaneously inoculated into the bilateral dorsal region of Balb/c nu/nu mice (3×10^6 cells/site). Luciferase-expressing MSCs (5×10^5 cells/body) were then administered through the left ventricular cavity (day 0). Luminescence was periodically measured through an intraperitoneal injection of D-luciferin (days 0–21). (d) Quantification of luminescence levels at the 9L tumor site after injection of VP-MSCs (□) or non-VP-MSCs (○). For each group, $n = 4$; $^*p < 0.05$ or $^{**}p < 0.01$ versus non-VP-MSC group. (e) Immunostaining for luciferase expression in the subcutaneous tumor. MSCs (5×10^5 cells/body) were injected into the left ventricular cavity immediately after subcutaneous inoculation of 9L cells in the bilateral dorsal part of the Balb/c nu/nu mice (day 0). The tumor tissues were obtained 21 days after MSC administration. Luciferase-positive cells (brown) were detected at the tumor periphery with an anti-luciferase antibody. Arrowheads, luciferase-positive cells. Scale bar = 100 mm

Table 2. Relative *luciferase* transgene copy number in 9L tumors in mice inoculated with VP-MSCs

		Relative *luciferase* transgene copy number	
		Experiment 1	Experiment 2
Central	Non-VP-MSCs.Luc	ND	ND
	VP-MSCs.Luc	ND	ND
Peripeheral	Non-VP-MSCs.Luc	1.0	1.0
	VP-MSCs.Luc	47.5	27.7

Small pieces of tissues were obtained from peripheral and central portions of tumors at 21 days after MSC administration. The relative copy number of the *luciferase* gene was determined as the ratio of the copy numbers in the peripheral portions of tumor in the group of 9L tumors inoculated with VP-MSCs to the copy numbers in non-VP-MSCs. The copy number of the reference gene *GAPDH* was also determined to correct for variation in the DNA amount and amplification efficiency.

of the mice (day 0), the luciferase expression peaked at day 10 and rapidly declined after day 14 (Figures 3a and 3b), indicating the elimination of inoculated MSCs. These results suggest that the signal enhancement after day 14 in the VP-MSC group was not caused by the expansion of inoculated MSCs.

Tumor-specific transduction by VP-MSCs

We evaluated the progeny retroviral transuduction of the tissues at 21 days after MSC administration. The 5′-LTR sequence of transgene in VP-MSCs and non-VP-MSCs does not contain the *Xba*I site (Figure 4a, upper panel). On the other hand, the 5′-LTR sequence of transgene in target cells transduced with progeny retrovirus produced from VP-MSCs contains the *Xba*I site because this 5′-LTR is the copy of 3′-LTR (containing the *Xba*I site) in retroviruses (Figure 4a, lower panel). Therefore, the presence of two fragments (440 bp + 120 bp) of PCR products from the 5′-LTR region (560 bp) indicates that retroviral vector-mediated gene transfer occurred. Because the PCR products from the tumors in the VP-MSC group were digested into two fragments with *Xba*I (Figure 4b), ths means that the tumors were transduced with progeny

DOI: 10.1002/jgm

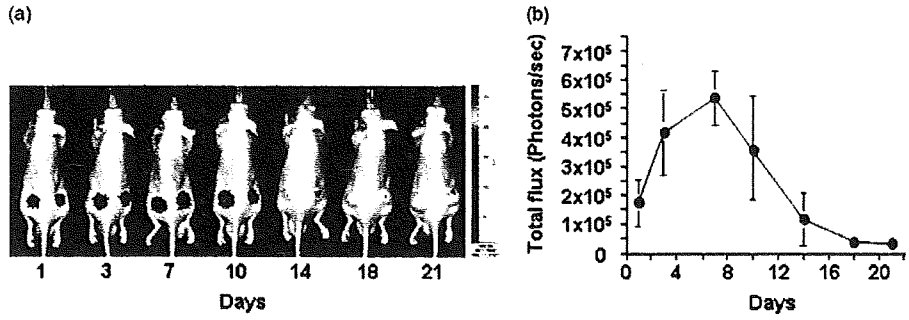

Figure 3. Survival of MSCs in subcutaneous 9L tumor. (a) Typical luminescence signals of luciferase-expressing MSCs measured using an *in vivo* imaging system. Stable luciferase-expressing MSCs mixed with an equal number of nontransduced 9L cells were subcutaneously inoculated into the bilateral dorsal region of nu/nu mice. (b) Time course of the quantified luminescence levels at tumor sites of the mice ($n = 4$)

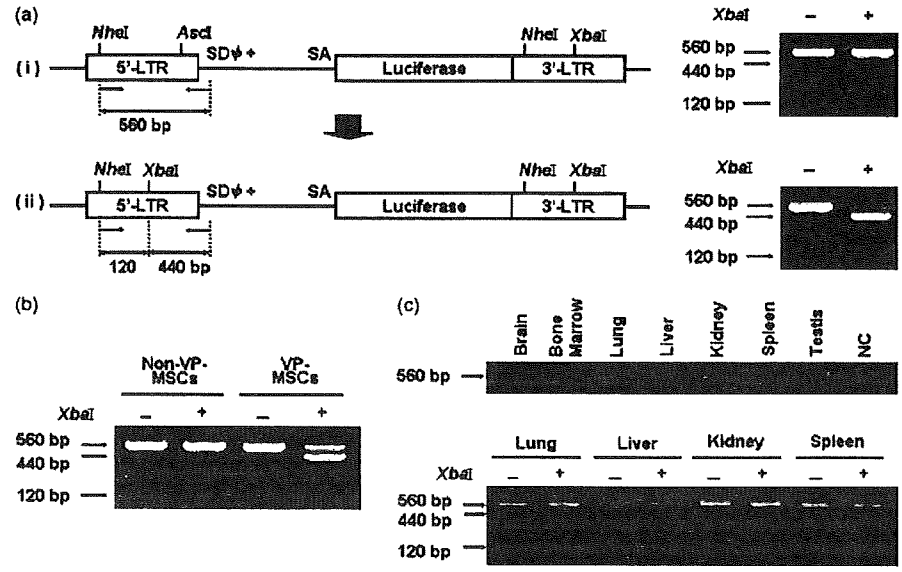

Figure 4. Tumor-specific transduction with progeny retroviral vectors in the VP-MSC system. (a) The diffrence in 5′-LTR sequences between MSCs (VP- and non-VP-) and target cells transduced with progeny retroviruses produced from VP-MSCs. The 5′-LTR sequence of transgene in VP-MSCs and non-VP-MSCs does not contain the *XbaI* site. On the other hand, the 5′-LTR sequence of transgene in target cells transduced with progeny retrovirus produced from VP-MSCs contains the *XbaI* site because this 5′-LTR is the copy of 3′-LTR (containing the *XbaI* site) in retroviruses. Therefore, the presence of two fragments (440 bp + 120 bp) after *XbaI* digestion of PCR products from the 5′-LTR region (560 bp) indicates that retroviral vector-mediated gene transfer occurred. (b) *XbaI* digestion pattern of the PCR products from the 5′-LTR region of the transgene in the tumor periphery at 21 days after MSC administration. The typical *XbaI* digested pattern indicates that transduction of the tumors with progeny retroviruses occurred. (c) The 5′-LTR region in the host tissues was examined by PCR/*XbaI* digestion at day 21 (upper panel). No typical *XbaI* digested pattern was observed in the normal tissues (lower panel), indicating the absence of retroviral vector-mediated gene transfer

retroviruses. In addition, normal tissues in the VP-MSC group were also examined PCR/*XbaI* digestion. Although the 5′-LTR region was amplified in several normal tissues (Figure 4c, upper panel), no typical *XbaI* digested pattern was observed, suggesting that gene transfer did not occur in such normal tissues/organs (Figure 4c, lower panel).

Anticancer effects of VP-MSCs *in vivo*

During the continuous infusion of GCV, tumor growth was significantly suppressed in the VP-MSC group compared to that in the non-VP-MSC, untransfected MSC or non-MSC control groups (Figure 5a). No difference in the tumor growth was observed without GCV administration (Figure 5b).

Discussion

In the present study, we developed MSCs that produce progeny retroviral vectors locally, which enable enhanced and tumor-specific transduction. Systemic delivery of modified MSCs enhanced transgene expression in the

DOI: 10.1002/jgm

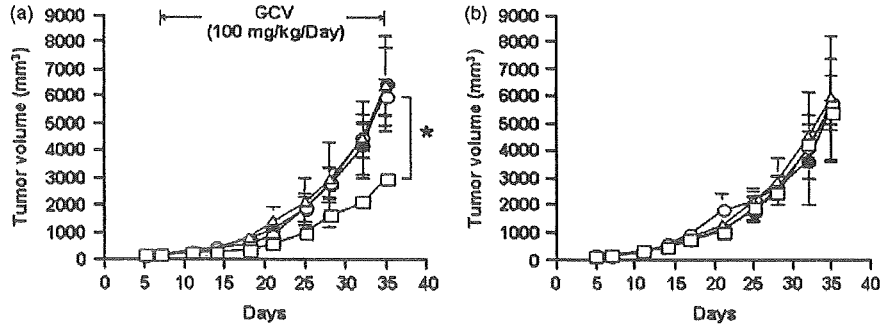

Figure 5. Anticancer effects of VP-MSCs *in vivo*. (a) Suppression of tumor growth after VP-MSC administration under GCV treatment. MSCs were injected into the left ventricular cavity immediately after subcutaneous inoculation of 9L cells into the bilateral dorsal region of Balb/c nu/nu mice (day 0). The mice were continuously administered GCV (100 mg/kg/d) from days 7–35 through intraperitoneal osmotic pumps. The tumor volume was measured periodically. (b) No change was observed in tumor growth without GCV treatment. The groups were: no MSCs (○); MSCs without genetic modification (●); MSCs nucleofected with an HSV-*tk*-expressing plasmid (non-VP-MSCs, Δ); and MSCs nucleofected with the retroviral vector components pLTR-*tk*, pGag-pol, and pVSV-G (VP-MSCs, □) ($n = 4$, for each group). *$p < 0.05$ versus non-VP-MSC group

9L tumors in mice. VP-MSC administration further augmented local transgene expression, leading to significant suppression of tumor growth compared to non-VP-MSC administration using a HSV-*tk*/GCV system.

Recently, nucleofection, an electroporation-based nonviral transfection technique, has been shown to be effective in transfection of MSCs [14]. In the present study, we found that nucleofection is also effective in preparing MSCs with a vector-producing property compared to other nonviral methods.

We demonstrated that systemic MSC administration enhanced transgene expression at the 9L tumor sites in mice, suggesting selective accumulation of MSCs at the tumor. Furthermore, the vector-producing property augmented amplification and expression of the luciferase gene *in vivo*. Immunostaining studies have demonstrated marked production of the luciferase protein at the tumors in the VP-MSC group. These results suggest that VP-MSCs can locally produce substantial amount of recombinant proteins not only through their homing ability, but also through the enhancement of transgene amplification and expression.

Our results may raise an important question about the origin of bioluminescence and immunostaining signals in the late phase: are the signals derived from VP-MSCs or transduced 9L cells? We demonstrated that most MSCs in the vicinity of 9L glioma cells were eliminated within 14 days *in vivo*. On the other hand, administration of VP-MSCs, but not non-VP-MSCs, further augmented the transgene expression at the tumor site after 14 days. These results suggest that luciferase signals in glioma at day 21 were mainly derived from 9L tumor cells transduced with progeny retroviral vectors.

The GCV-dependent anticancer effect and *tk* gene amplification in the VP-MSC group was significantly greater than that in the non-VP-MSC group *in vitro*. The IC_{50} value of GCV when it was used in concert with VP-MSCs was far lower (approximately 1 : 250) than when it was used with non-VP-MSCs. This anticancer effect of HSV-*tk*-expressing VP-MSCs *in vivo* was considered to be due to TK expression, and not due to the oncolytic properties of the progeny retrovirus because no anticancer effect was observed in the VP-MSC group without GCV treatment.

Although the effect of VP-MSCs was significantly greater than that of non-VP-MSCs, it was still partial. MSCs are suitable for repeated administration because they have little immunogenicity due to the lack of costimulatory molecule expression [7,15–17]. In addition, in the present study, VP-MSCs were administered on the same day of tumor cell inoculation. In our preliminary data, VP-MSCs have limited therapeutic effects on established palpable 9L tumor (data not shown). Preferential accumulation of VP-MSCs at the tumor periphery may explain their partial anticancer effects. Repeated administration of VP-MSCs would also be required for the treatment of established tumors.

Finally, we assessed the biodistribution and replication of progeny retrovirus to ensure the safety and specificity of our system. In the present study, after 21 days of systemic VP-MSC administration, PCR analysis revealed weak amplification of a 5′-LTR sequence in the bone marrow, lungs, kidneys and spleen. When the non-VP- and VP-MSCs were inoculated into the tumor-bearing mice, an IVIS imaging study showed that definite gene expression from MSCs was limited to the tumor site (Figures 2b and 2c). VP-MSCs expressing HSV-*tk* are considered to localize to tumor tissues in the same way. Although a small amount of transgene was detected in several normal tissues by PCR analysis, the *Xba*I-digestion pattern revealed that the transgene was derived from inoculated MSCs (Figure 4c). These results indicate that, even if a small number of injected VP-MSCs were remained in normal tissues, transduction by progeny retrovirus did not occur in these normal tissues. On the other hand, the PCR/*Xba*I digestion experiments showed that retrovirus-mediated gene transfer occurred in the vicinity of tumors. These results ensure the safety and tumor-specific transduction of the VP-MSC system.

DOI: 10.1002/jgm

In conclusion, this is the first study to demonstrate the effectiveness and safety of systemic administration of VP-MSCs in tumor-bearing mice. VP-MSCs exert their function through *in situ* retroviral vector production and expression of transgenes after accumulation at tumors. Although our system needs to be improved further, the present findings will contribute to the development of more efficient cancer gene therapy using MSCs as a platform.

Acknowledgements

We wish to thank Dr Masafumi Onodera for providing pLTR, pGP and pVSVG. This study was supported in part by Grants-in-aid for Scientific Research; a grant from the 21st Century COE Program; the 'High-Tech Research Center' Project for Private Universities, matching fund subsidy from the Ministry of Education, Culture, Sports, and Technology of Japan; and the Inoue Enryo Memorial Foundation for Promoting Science.

References

1. Ram Z, Culver KW, Oshiro EM, *et al.* Therapy of malignant brain tumors by intratumoral implantation of retroviral vector-producing cells. *Nat Med* 1997; **3**: 1354–1361.
2. Rainov NG. A phase III clinical evaluation of herpes simplex virus type 1 thymidine kinase and ganciclovir gene therapy as an adjuvant to surgical resection and radiation in adults with previously untreated glioblastoma multiforme. *Hum Gene Ther* 2000; **11**: 2389–2401.
3. Hall B, Dembinski J, Sasser AK, *et al.* Mesenchymal stem cells in cancer: tumor-associated fibroblasts and cell-based delivery vehicles. *Int J Hematol* 2007; **86**: 8–16.
4. Nakamizo A, Marini F, Amano T, *et al.* Human bone marrow-derived mesenchymal stem cells in the treatment of gliomas. *Cancer Res* 2005; **65**: 3307–3318.
5. Ozawa K, Sato K, Oh I, *et al.* Cell and gene therapy using mesenchymal stem cells (MSCs). *J Autoimmun* 2008; **30**: 121–127.
6. Karnoub AE, Dash AB, Vo AP, *et al.* Mesenchymal stem cells within tumour stroma promote breast cancer metastasis. *Nature* 2007; **449**: 557–563.
7. Maitra B, Szekely E, Gjini K, *et al.* Human mesenchymal stem cells support unrelated donor hematopoietic stem cells and suppress T-cell activation. *Bone Marrow Transplant* 2004; **33**: 597–604.
8. Hanahan D, Weinberg RA. The hallmarks of cancer. *Cell* 2000; **100**: 57–70.
9. Hall B, Andreeff M, Marini F. The participation of mesenchymal stem cells in tumor stroma formation and their application as targeted-gene delivery vehicles. *Handb Exp Pharmacol* 2007; 263–283.
10. Le Blanc K, Ringden O. Immunobiology of human mesenchymal stem cells and future use in hematopoietic stem cell transplantation. *Biol Blood Marrow Transplant* 2005; **11**: 321–334.
11. Studeny M, Marini FC, Champlin RE, *et al.* Bone marrow-derived mesenchymal stem cells as vehicles for interferon-beta delivery into tumors. *Cancer Res* 2002; **62**: 3603–3608.
12. Okada T, Caplen NJ, Ramsey WJ, *et al.* In situ generation of pseudotyped retroviral progeny by adenovirus-mediated transduction of tumor cells enhances the killing effect of HSV-tk suicide gene therapy in vitro and in vivo. *J Gene Med* 2004; **6**: 288–299.
13. Nakamura K, Ito Y, Kawano Y, *et al.* Antitumor effect of genetically engineered mesenchymal stem cells in a rat glioma model. *Gene Ther* 2004; **11**: 1155–1164.
14. Aluigi M, Fogli M, Curti A, *et al.* Nucleofection is an efficient nonviral transfection technique for human bone marrow-derived mesenchymal stem cells. *Stem Cells* 2006; **24**: 454–461.
15. Aggarwal S, Pittenger MF. Human mesenchymal stem cells modulate allogeneic immune cell responses. *Blood* 2005; **105**: 1815–1822.
16. Le Blanc K, Rasmusson I, Sundberg B, *et al.* Treatment of severe acute graft-versus-host disease with third party haploidentical mesenchymal stem cells. *Lancet* 2004; **363**: 1439–1441.
17. Barry FP, Murphy JM, English K, *et al.* Immunogenicity of adult mesenchymal stem cells: lessons from the fetal allograft. *Stem Cells Dev* 2005; **14**: 252–265.

nature Vol 460 13 August 2009 doi:10.1038/nature08240

LETTERS

Gain-of-function of mutated *C-CBL* tumour suppressor in myeloid neoplasms

Masashi Sanada[1,5]*, Takahiro Suzuki[7]*, Lee-Yung Shih[8]*, Makoto Otsu[9], Motohiro Kato[1,2], Satoshi Yamazaki[6], Azusa Tamura[1], Hiroaki Honda[11], Mamiko Sakata-Yanagimoto[12], Keiki Kumano[3], Hideaki Oda[13], Tetsuya Yamagata[14], Junko Takita[1,2,3], Noriko Gotoh[10], Kumi Nakazaki[1,4], Norihiko Kawamata[15], Masafumi Onodera[16], Masaharu Nobuyoshi[7], Yasuhide Hayashi[17], Hiroshi Harada[18], Mineo Kurokawa[3,4], Shigeru Chiba[12], Hiraku Mori[18], Keiya Ozawa[7], Mitsuhiro Omine[18], Hisamaru Hirai[3,4], Hiromitsu Nakauchi[6,9], H. Phillip Koeffler[15] & Seishi Ogawa[1,5]

Acquired uniparental disomy (aUPD) is a common feature of cancer genomes, leading to loss of heterozygosity. aUPD is associated not only with loss-of-function mutations of tumour suppressor genes[1], but also with gain-of-function mutations of proto-oncogenes[2]. Here we show unique gain-of-function mutations of the *C-CBL* (also known as *CBL*) tumour suppressor that are tightly associated with aUPD of the 11q arm in myeloid neoplasms showing myeloproliferative features. The *C-CBL* proto-oncogene, a cellular homologue of *v-Cbl*, encodes an E3 ubiquitin ligase and negatively regulates signal transduction of tyrosine kinases[3–6]. Homozygous *C-CBL* mutations were found in most 11q-aUPD-positive myeloid malignancies. Although the *C-CBL* mutations were oncogenic in NIH3T3 cells, c-Cbl was shown to functionally and genetically act as a tumour suppressor. C-CBL mutants did not have E3 ubiquitin ligase activity, but inhibited that of wild-type C-CBL and CBL-B (also known as CBLB), leading to prolonged activation of tyrosine kinases after cytokine stimulation. *c-Cbl*$^{-/-}$ haematopoietic stem/progenitor cells (HSPCs) showed enhanced sensitivity to a variety of cytokines compared to *c-Cbl*$^{+/+}$ HSPCs, and transduction of *C-CBL* mutants into *c-Cbl*$^{-/-}$ HSPCs further augmented their sensitivities to a broader spectrum of cytokines, including stem-cell factor (SCF, also known as KITLG), thrombopoietin (TPO, also known as THPO), IL3 and FLT3 ligand (FLT3LG), indicating the presence of a gain-of-function that could not be attributed to a simple loss-of-function. The gain-of-function effects of C-CBL mutants on cytokine sensitivity of HSPCs largely disappeared in a *c-Cbl*$^{+/+}$ background or by co-transduction of wild-type *C-CBL*, which suggests the pathogenic importance of loss of wild-type *C-CBL* alleles found in most cases of *C-CBL*-mutated myeloid neoplasms. Our findings provide a new insight into a role of gain-of-function mutations of a tumour suppressor associated with aUPD in the pathogenesis of some myeloid cancer subsets.

Myelodysplastic syndromes (MDS) are heterogeneous groups of blood cancers originating from haematopoietic precursors. They are characterized by deregulated haematopoiesis showing a high propensity to acute myeloid leukaemia (AML)[7]. Some MDS cases have overlapping clinico-pathological features with myeloproliferative disorders, and are now classified into myelodysplasia/myeloproliferative neoplasms (MDS/MPN) by the World Health Organization (WHO) classification[8]. To obtain a comprehensive profile of allelic imbalances in these myeloid neoplasms, we performed allele-specific copy number analyses of bone marrow samples obtained from 222 patients with MDS, MDS/MPN, or other related myeloid neoplasms (Supplementary Tables 1 and 2) using high-density single nucleotide polymorphism (SNP) arrays combined with CNAG/AsCNAR software[9,10].

Genomic profiles of MDS and MDS/MPN showed characteristic unbalanced genetic changes, as reported in previous cytogenetic studies[11] (Supplementary Fig. 1a); however, they were detected more sensitively by SNP array analyses (Supplementary Table 3). aUPD was detected in 70 samples (31.5%) on the basis of the allele-specific copy number analyses, which substantially exceeded the detection rate obtained using a SNP call-based detection algorithm (20.7%) (Supplementary Figs 2 and 4, and Supplementary Tables 4 and 5). Long stretches of homozygous SNP calls caused by shared identical-by-descent alleles in parents were empirically predicted and excluded (Supplementary Fig. 3). aUPDs were more common in MDS/MPN than in MDS. They preferentially affected several chromosomal arms (1p, 1q, 4q, 7q, 11p, 11q, 14q, 17p and 21q) in distinct subsets of patients, and frequently associated with mutated oncogenes and tumour suppressor genes (Supplementary Figs 1b and 5). Among these, the most common aUPDs were those involving 11q ($n = 17$), which defined a unique subset of myeloid neoplasms that were clinically characterized by frequent diagnosis of chronic myelomonocytic leukaemia (CMML) with normal karyotypes (13 cases) (Fig. 1a and Supplementary Table 6). We identified a minimum overlapping aUPD segment of approximately 1.4 megabases (Mb) in 11q, which contained a mutated *C-CBL* proto-oncogene (Fig. 1b).

[1]Cancer Genomics Project, [2]Department of Pediatrics, [3]Cell Therapy and Transplantation Medicine, and [4]Hematology and Oncology, Graduate School of Medicine, The University of Tokyo, 7-3-1 Hongo, Bunkyo-ku, Tokyo 113-8655, Japan. [5]Core Research for Evolutional Science and Technology, [6]Exploratory Research for Advanced Technology, Japan Science and Technology Agency, 4-1-8 Honcho, Kawaguchi-shi, Saitama 332-0012, Japan. [7]Division of Hematology, Department of Medicine, Jichi Medical University, 3311-1 Yakushiji, Shimotsuke-shi, Tochigi 329-0498, Japan. [8]Division of Hematology-Oncology, Department of Internal Medicine, Chang Gung Memorial Hospital, Chang Gung University, 199 Tung Hwa North Road, Taipei 105, Taiwan. [9]Division of Stem Cell Therapy, Center for Stem Cell and Regenerative Medicine, [10]Division of Systems Biomedical Technology, Institute of Medical Science, The University of Tokyo, 4-6-1 Shirokanedai, Minato-ku, Tokyo 108-8639, Japan. [11]Department of Developmental Biology, Research Institute of Radiation Biology and Medicine, Hiroshima University, 1-2-3 Kasumi, Minami-ku, Hiroshima 734-8553, Japan. [12]Department of Clinical and Experimental Hematology, Institute of Clinical Medicine, University of Tsukuba, 1-1-1 Tennodai, Tukuba-shi, Ibaraki, 305-8571, Japan. [13]Department of Pathology, Tokyo Women's Medical University, 8-1 Kawada-cho, Shinjuku-ku, Tokyo 162-8666, Japan. [14]Department of Hematology, Dokkyo University School of Medicine, 800 Kitabayashi, Mibu, Tochigi 321-0293, Japan. [15]Hematology/Oncology, Cedars-Sinai Medical Center, 8700 Beverly Boulevard, Los Angeles, California 90048, USA. [16]Department of Genetics, National Research Institute for Child Health and Development, 2-10-1 Okura, Setagaya-ku, Tokyo, 157-8535, Japan. [17]Gunma Children's Medical Center, 779 Shimohakoda, Hokkitsu-machi, Shibukawa-shi, Gunma 377-8577, Japan. [18]Division of Hematology, Internal Medicine, Showa University Fujigaoka Hospital, 1-30 Fujigaoka, Aoba-ku, Yokohama, Kanagawa 227-8501, Japan.
*These authors contributed equally to this work.

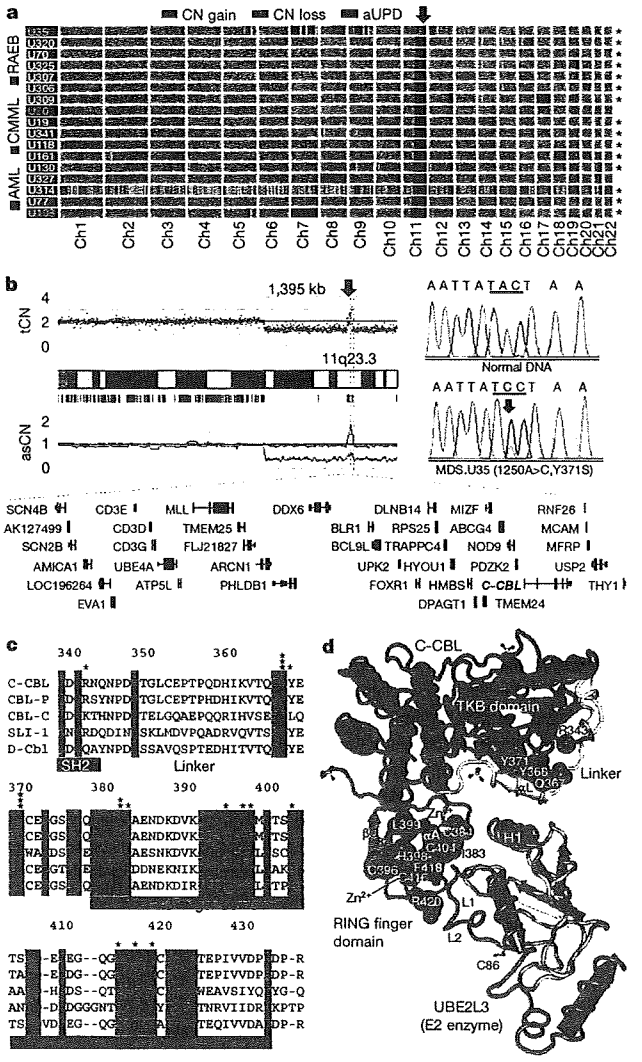

Figure 1 | Common UPD on the 11q arm and *C-CBL* mutations in myeloid neoplasms. **a**, Copy number profiles of 17 cases with myeloid neoplasms showing 11qUPD. Regions of copy number (CN) gains, losses and aUPD are depicted in different colours. Histologies are shown by coloured boxes. Asterisks denote *C-CBL*-mutated cases. Ch, chromosome; RAEB, refractory anaemia with excess blasts. **b**, CNAG output for MDS.U35. Total copy number (tCN) and allele-specific copy number (asCN) plots show a focal copy number gain spanning a 1.4-Mb segment within 3 Mb of an 11q-aUPD region (left), which contained mutated *C-CBL* in MDS.U35 (right). **c**, Alignments of amino acid sequences for human CBL family proteins and their homologues in *Caenorhabditis elegans* (SLI-1) and *Drosophila* (D-Cbl). Amino acid numbering is on the basis of human *C-CBL*. Conserved amino acids are highlighted. Positions of mutated amino acids are indicated by asterisks. Heterozygous mutations are shown in red. **d**, Mutated amino acid positions in the three-dimensional structure of a human C-CBL–UBE2L3 complex. TKB, tyrosine kinase binding domain.

C-CBL is the cellular homologue of the *v-Cbl* transforming gene of the Cas NS-1 murine leukaemia virus[5,12]. It was recently found to be mutated in human AML cases[13–15]. Together with its close homologue, CBL-B, C-CBL is thought to be involved in the negative modulation of tyrosine kinase signalling, primarily through their E3 ubiquitin ligase activity that is responsible for the downregulation of activated tyrosine kinases[3–5]. By sequencing all *C-CBL* exons in all 222 samples, we found *C-CBL* mutations in 15 of the 17 cases with 11q-aUPD, whereas only 3 out of 205 cases without 11q-aUPD had *C-CBL* mutations, showing a strong association of *C-CBL* mutations with 11q-aUPD ($P = 1.46 \times 10^{-18}$) (Supplementary Fig. 6 and Supplementary Tables 6 and 7), as also indicated in a recent report[16]. Thus, *C-CBL* was thought to be the major, if not the only, target of 11q-aUPD in myeloid neoplasms. Two different *C-CBL* mutations co-existed in three cases (Supplementary Fig. 6b). Somatic origins of the mutations were confirmed in three evaluable cases (Supplementary Fig. 6c).

In most cases, *C-CBL* mutations were missense, involving the evolutionarily conserved amino acids within the linker-RING finger domain that is central to the E3 ubiquitin ligase activity[17] (Fig. 1c). Another case with a predominant Cys384Tyr mutation also contained a nonsense mutation (Arg343X) in a minor subclone, which resulted in a v-Cbl-like truncated protein (Supplementary Fig. 6b). In the remaining two cases, mutations led to amino acid deletions (Δ369−371 and Δ368−382) involving the highly conserved α-helix (αL) of the linker domain and the first loop of the RING finger. According to the published crystal structure of *C-CBL*[17], most of the mutated or deleted amino acids were positioned on the interface for the binding to the E2 enzyme (Fig. 1d), making contact with either the tyrosine kinase binding domain (Tyr 368 and Tyr 371) or E2 ubiquitin-conjugating enzymes (Ile 383, Cys 404 and Phe 418). Especially, all seven linker-domain mutations selectively involved just three amino acids (Gln 367, Tyr 368 and Tyr 371) within the conserved αL helix (Fig. 1d). Mutations were clearly homozygous in nine cases, and the apparently heterozygous chromatograms in the other six cases could also be compatible with homozygous mutations affecting the aUPD-positive tumour clones, given the presence of substantial normal cell components within these samples. Mutations in the remaining three cases were considered to be heterozygous. About half of the *C-CBL*-mutated cases carried coexisting mutations of *RUNX1* (four cases), *TP53* (one case), *FLT3* internal tandem duplication (1 case) or *JAK2* (3 cases). *NRAS* and *KRAS* mutations were prevalent among CMML (15.1%) but occurred within discrete clusters from *C-CBL*-mutated cases (Supplementary Tables 2 and 6 and Supplementary Fig. 5). The mutation status of *C-CBL* did not substantially affect the clinical outcome (Supplementary Fig. 7).

All tested *C-CBL* mutants induced clear oncogenic phenotypes in NIH3T3 fibroblasts, as demonstrated by enhanced colony formation in soft agar and tumour generation in nude mice (Supplementary Fig. 8). Transformed NIH3T3 cells showed PI3 kinase-dependent activation of Akt and the transformed phenotype was reverted by treatment with the PI3 kinase inhibitor Ly294002 (Supplementary Fig. 9). When introduced into $Lin^-Sca1^+c\text{-}Kit^+$ (LSK) HSPCs, C-CBL mutants (C-CBL(Gln367Pro) and C-CBL(Tyr371Ser)), as well as a mouse lymphoma-derived oncogenic mutant (C-CBL(70Z)), significantly promoted the replating capacity of these progenitors (Fig. 2a). Because c-Cbl negatively modulates tyrosine kinase signalling, and all *C-CBL* mutations, including those previously reported[13–16], affected the critical domains for its enzymatic activity involved in this modulation, C-CBL was postulated to have a tumour suppressor function; loss-of-function could be a mechanism for the oncogenicity of these C-CBL mutants[3,5]. To assess this possibility and to clarify further the role of *C-CBL* mutations in the pathogenesis of myeloid neoplasms, we generated *c-Cbl*$^{-/-}$ mice and examined their haematological phenotypes (Supplementary Fig. 10).

In agreement with previous reports[18–20], *c-Cbl*$^{-/-}$ mice exhibited splenomegaly and an augmented haematopoietic progenitor pool, as was evident from the increased colony formation of bone marrow cells in methylcellulose culture and higher numbers of LSK and CD34-negative LSK cells in bone marrow and/or spleen compared to their wild-type littermates (Fig. 2b–d and Supplementary Fig. 11). Furthermore, when introduced into a *BCR-ABL* transgenic background[21], the *c-Cbl*$^{-/-}$ allele accelerated blastic crisis depending on the allele dosage (Fig. 2e, f). These observations supported the notion that wild-type *C-CBL* has tumour suppressor functions, whereas 'mutant' *C-CBL* acts as an oncogene; *C-CBL* can therefore be both a proto-oncogene and a tumour suppressor gene.

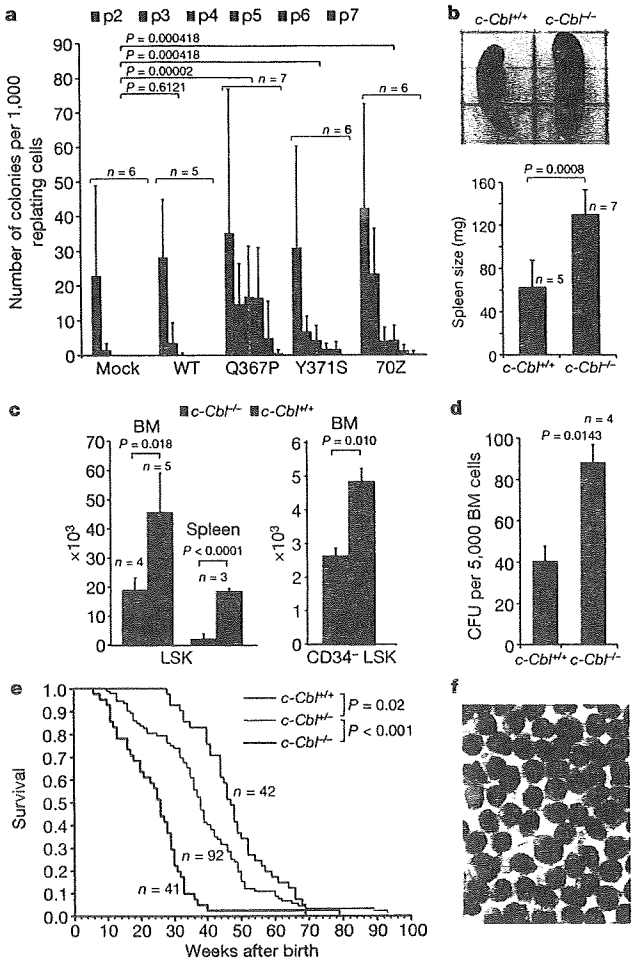

Figure 2 | Tumour-suppressor functions of wild-type C-CBL. **a**, Prolonged replating capacity of LSK cells transduced with mutant *C-CBL* (*C-CBL*(Gln367Pro) and *C-CBL*(Tyr371Ser)), compared to mock- or wild-type *C-CBL*-transduced cells. Replating capacity in methylcellulose culture is shown as mean colony number (and s.d.) per 1,000 replating cells at indicated times of replating. p, passage. **b**, Increased spleen mass in *c-Cbl*$^{-/-}$ mice compared to *c-Cbl*$^{+/+}$ mice (mean spleen weight and s.d.). **c**, Mean number of total LSK (left) and CD34-negative LSK (right) cells (plus s.d.) in bone marrow (BM) and/or spleen in *c-Cbl*$^{+/+}$ (blue columns) and *c-Cbl*$^{-/-}$ mice (red columns). Bone marrow cells from bilateral tibias and femurs were counted for each mouse. **d**, Augmented colony-forming potential of bone marrow cells from *c-Cbl*$^{-/-}$ mice (mean colony number and s.d. per 5,000 bone marrow cells). CFU, colony-forming units. **e**, Kaplan–Meier survival curves of *c-Cbl*$^{+/+}$, *c-Cbl*$^{+/-}$ and *c-Cbl*$^{-/-}$ mice carrying a *BCR-ABL* transgene, showing acceleration of blastic crisis in *c-Cbl*$^{+/-}$ and *c-Cbl*$^{-/-}$ mice. **f**, Wright–Giemsa staining of an enlarged lymph node in a *Bcr-Abl*$^{+}$ *c-Cbl*$^{-/-}$ mouse during blastic crisis shows massive infiltrates of immature leukaemic blasts. Original magnification, ×600.

Mouse LSK HSPCs expressed two Cbl family member proteins: wild-type c-Cbl and Cbl-b (Supplementary Fig. 12)[22]. When transduced into NIH3T3 cells stably expressing human epidermal growth factor receptor (EGFR), both Cbl proteins enhanced ubiquitination of EGFR after EGF stimulation, which was suppressed by coexpression of the C-CBL mutants (Fig. 3a, b). In haematopoietic cells, overexpression of wild-type C-CBL enhanced ligand-induced ubiquitination of a variety of tyrosine kinases, including c-KIT, FLT3 and JAK2. In contrast, C-CBL mutants not only showed compromised enzymatic activity, but also inhibited the ubiquitinating activities in these haematopoietic cells (Fig. 3c), leading to prolonged tyrosine kinase activation after ligand stimulation (Fig. 3d).

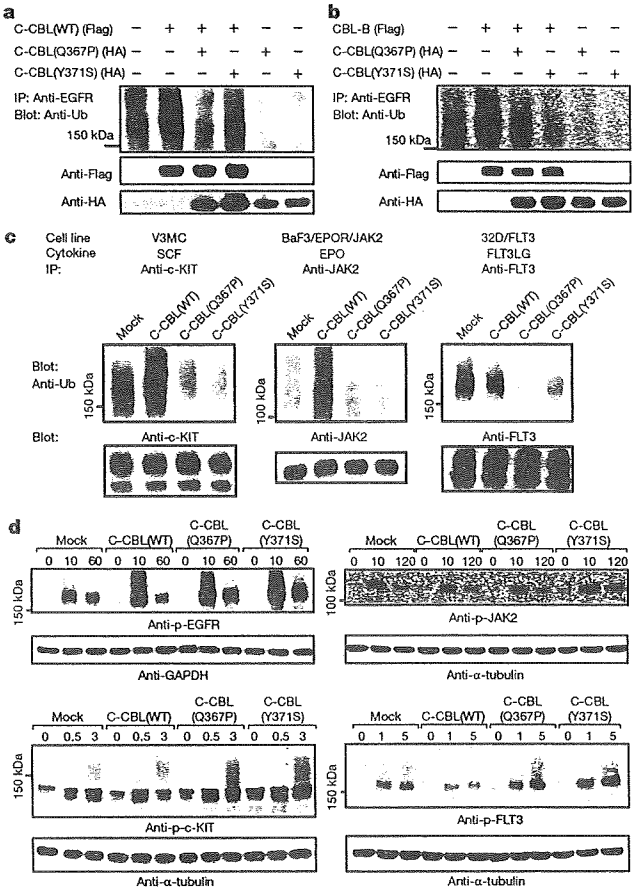

Figure 3 | Inhibitory actions of C-CBL mutants on wild-type C-CBL. **a**, **b**, Flag-tagged wild-type C-CBL (**a**) or CBL-B (**b**) were transfected into NIH3T3 cells stably transduced with human EGFR plus indicated HA-tagged C-CBL mutants. Anti-ubiquitin blots of immunoprecipitated EGFR after EGF stimulation show the inhibitory actions of the C-CBL mutants on ubiquitinating activity of C-CBL (**a**) and CBL-B (**b**). Bottom panels are anti-HA and anti-Flag blots of total cell lysates. **c**, Effects of wild-type and mutant C-CBL on cytokine-induced ubiquitination of c-KIT, JAK2 and FLT3 in haematopoietic cells V3MC, BaF3 co-transduced with human erythropoietin receptor (EPOR) and JAK2 (BaF3/EPOR/JAK2), and FLT3-transduced 32D (32D/FLT3), respectively. Each cell line was further transduced with indicated C-CBL mutants, and ubiquitination of immunoprecipitated kinases was detected by anti-ubiquitin blots at 1 min after stimulation with SCF, EPO and FLT3LG. Anti-kinase blots of the precipitated kinases are shown below each panel. **d**, Kinase phosphorylation was examined at indicated time points (shown in minutes) after ligand stimulation using immunoblot analyses of total cell lysates using antibodies to phosphorylated (p-) EGFR, c-KIT, JAK2 and FLT3 in which anti-α-tubulin or anti-GAPDH blots are provided as a control.

Because tyrosine kinase signalling is central to cytokine responses in haematopoietic cells and its deregulation is a common feature of myeloproliferative disorders[23], we next examined the effects of *C-CBL* mutations (*C-CBL*(Gln367Pro) and *C-CBL*(Tyr371Ser)) and the loss of wild-type *C-CBL* alleles on the responses of LSK HSPCs to various cytokines. In serum-free conditions, *c-Cbl*$^{-/-}$ LSK cells showed a modestly enhanced proliferative response to a variety of cytokines, including SCF, IL3 and TPO, compared to *c-Cbl*$^{+/+}$ cells (mock columns in Fig. 4a). However, the enhanced response in *c-Cbl*$^{-/-}$ cells was markedly augmented and extended to a broader spectrum of cytokines, including FLT3 ligand by the transduction of *C-CBL* mutants. Of note, the effect of *C-CBL* mutant transduction was not remarkable in *c-Cbl*$^{+/+}$ LSK cells except for the response to SCF, which was clearly enhanced by *C-CBL* mutants

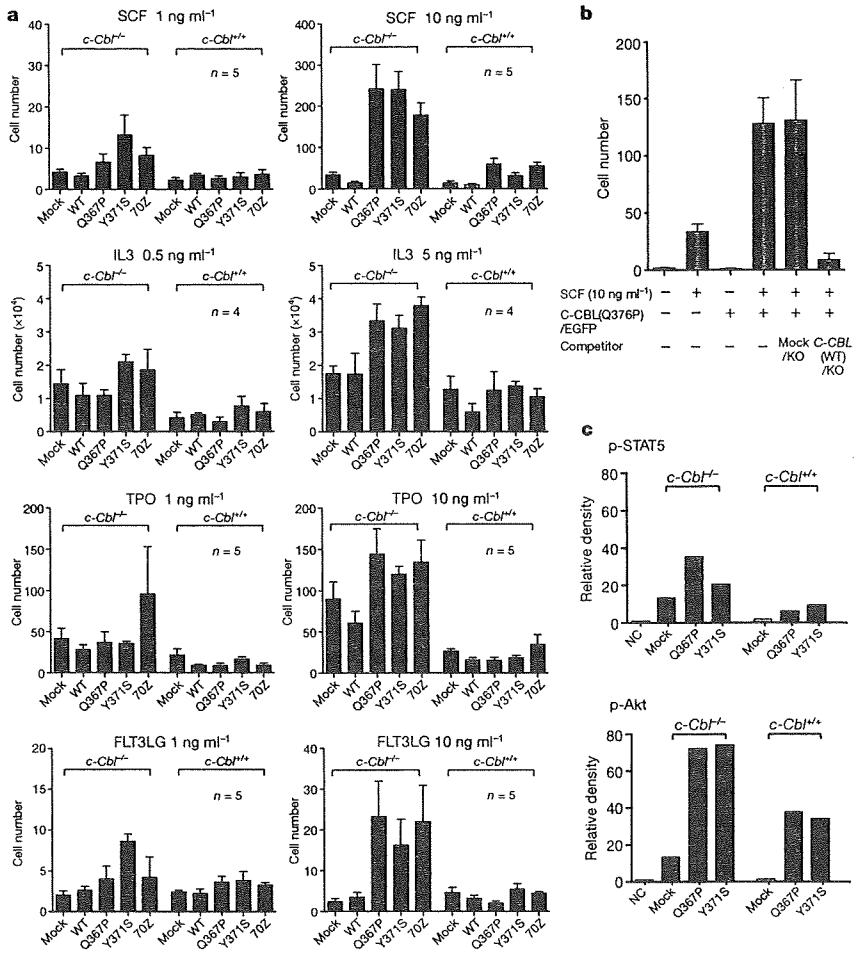

Figure 4 | Gain-of-function of mutant C-CBL augmented by loss of wild-type C-CBL. **a**, *c-Cbl*$^{+/+}$ and *c-Cbl*$^{-/-}$ LSK cells were transfected with various *C-CBL* internal ribosome entry site (IRES)/green fluorescent protein (GFP) constructs, and 50 GFP-positive cells were sorted for serum-free culture containing indicated concentrations of SCF, IL3, TPO and FLT3LG. Mean cell numbers (plus s.e.m.) on day 5 are plotted. **b**, *c-Cbl*$^{-/-}$ LSK cells were co-transduced with C-CBL(Gln367Pro)-IRES-EGFP (C-CBL(Q367P)/EGFP) and mock-IRES-Kusabira-Orange (mock/KO) or wild-type *C-CBL*-IRES-Kusabira-Orange (*C-CBL*(WT)/KO), and 50 GFP/KO double-positive cells were sorted into each well for cell proliferation assays in serum-free culture containing 10 ng ml^{-1} SCF. Mean cell numbers on day 5 (plus s.e.m., $n = 5$) are plotted. **c**, Ten thousand *c-Cbl*$^{+/+}$ and *c-Cbl*$^{-/-}$ LSK cells transduced with various C-CBL constructs were stimulated with 10 ng ml^{-1} SCF and 10 ng ml^{-1} TPO for 15 min. Total cell lysates were analysed by immunoblotting, using antibodies to STAT5, Akt and their phosphorylated forms. The intensities of phosphorylated proteins relative to total STAT5 (top panel) and Akt (bottom panel) are plotted. NC indicates the mean background signal obtained with nonspecific IgG.

even with a *c-Cbl*$^{+/+}$ background (Fig. 4a and Supplementary Fig. 13). To clarify further the effect of wild-type C-CBL on C-CBL mutants, both wild-type C-CBL and C-CBL mutants were co-transduced into *c-Cbl*$^{-/-}$ LSK cells, and their effects on the response to SCF were examined. As shown in Fig. 4b, the hyperproliferative response induced by C-CBL mutants was almost completely abolished by the co-transduction of wild-type C-CBL, suggesting the pathogenic importance of loss of wild-type *C-CBL* alleles found in most *C-CBL*-mutated cases. LSK cells transduced with C-CBL mutants also showed enhanced activation of the STAT5 and Akt pathways on cytokine stimulation (SCF and TPO), which was more pronounced in *c-Cbl*$^{-/-}$ than *c-Cbl*$^{+/+}$ LSK cells (Fig. 4c and Supplementary Fig. 14).

The modest enhancement of sensitivity to cytokines found in *c-Cbl*$^{-/-}$ LSK cells was a consequence of loss of C-CBL functions. In contrast, the hypersensitive response of mutant-transduced *c-Cbl*$^{-/-}$ LSK cells to a broad spectrum of cytokines represents gain-of-function of the mutants that could not be ascribed to a simple loss of C-CBL functions, which was also predicted from the strong association of *C-CBL* mutations with 11q-aUPD by analogy to the gain-of-function *JAK2* mutations associated with 9p-aUPD in polycythemia vera[2]. The gain-of-function of C-CBL mutants became more evident under a *c-Cbl*$^{-/-}$ background. The hypersensitive response to cytokines induced by mutant C-CBL under the *c-Cbl*$^{-/-}$ background was largely offset by the presence of the wild-type *c-Cbl* allele or by the transduction of the wild-type C-CBL gene, suggesting that the gain-of-function could be closely related to loss of C-CBL-like functions, probably by inhibition of Cbl-b. Supporting this view is a previous report that *c-Cbl/Cbl-b* double knockout T cells showed more profound impairments in the downregulation of the T-cell receptor (TCR), more sustained TCR signalling, and more vigorous proliferation, than *c-Cbl* or *Cbl-b* single knockout T cells after anti-CD3 (also known as CD3e) stimulation[24]. This is analogous to the gain-of-function found in some TP53 mutants, which has been explained by functional inhibition of two TP53 homologues, TP73 and TP63 (refs 25, 26). Of note, TP53 was also originally isolated as an oncogene through its mutated forms[27]. The Cbl-b inhibition-based gain-of-function model could be tested directly by comparing the behaviour of *c-Cbl/Cbl-b* double knockout LSK cells with that of LSK cells carrying homozygously knocked-in mutant *C-CBL* alleles. On the other hand, there remains a possibility that the gain-of-function could be mediated by a mechanism other than the simple inhibition of the homologue, because C-CBL mutants retained several motifs

that interacted with numerous signal-transducing molecules. Furthermore, considering the ubiquitous expression of CBL proteins, it would be of interest to explore the possible involvement of mutations in all *CBL* family members in other human cancers.

METHODS SUMMARY

Genomic DNA from 222 bone marrow samples with myeloid neoplasms were analysed using GeneChip SNP-genotyping microarrays (Affymetrix GeneChip) as described[28]. Allelic imbalances were detected from the allele-specific copy numbers calculated using CNAG/AsCNAR software (http://www.genome.umin.jp)[9,10]. *C-CBL* mutations were examined by sequencing PCR-amplified genomic DNA. For functional assays, haemagglutinin (HA)- or Flag-tagged complementary DNAs of wild-type and mutant *C-CBL* were generated by *in vitro* mutagenesis, constructed into a MSCV-based retroviral vector, pGCDNsamIRESGFP or pGCDNsamIRESKO, and used for retrovirus-mediated gene transfer. For the evaluation of oncogenicity of C-CBL mutants, NIH3T3 cells were transfected with various *C-CBL* constructs and used for colony assays in soft agar and tumour formation assays in nude mice. *c-Cbl*-deficient mice were generated using a conventional strategy of gene-targeting and crossed with *BCR-ABL* transgenic mice to evaluate the effect of the $c\text{-}Cbl^{-}$ allele on the acceleration of blastic crisis. LSK cells sorted from $c\text{-}Cbl^{+/+}$ and $c\text{-}Cbl^{-/-}$ mice were transduced with various *C-CBL* constructs. Their responses to cytokines were evaluated by cell proliferation assays, followed by immunoblot analyses of c-KIT, FLT3 and JAK2, as well as their downstream signalling molecules. The effects of C-CBL mutant expression on the ubiquitination of EGFR, c-KIT, FLT3 and JAK2 were examined by transducing C-CBL mutants into relevant cells, followed by anti-ubiquitin blots of the immunoprecipitated kinases after ligand stimulation. Functional competition of C-CBL mutants with wild-type C-CBL was assessed by cell proliferation assays of LSK cells co-transduced with both wild-type and mutant C-CBL genes. This study was approved by the ethics boards of the University of Tokyo, Chang Gung Memorial Hospital and Showa University. Antibodies and primers used in this study are listed in Supplementary Tables 8 and 9.

Full Methods and any associated references are available in the online version of the paper at www.nature.com/nature.

Received 9 October 2008; accepted 30 June 2009.
Published online 20 July 2009.

1. Knudson, A. G. Two genetic hits (more or less) to cancer. *Nature Rev. Cancer* 1, 157–162 (2001).
2. James, C. *et al.* A unique clonal JAK2 mutation leading to constitutive signalling causes polycythaemia vera. *Nature* 434, 1144–1148 (2005).
3. Ryan, P. E. *et al.* Regulating the regulator: negative regulation of Cbl ubiquitin ligases. *Trends Biochem. Sci.* 31, 79–88 (2006).
4. Schmidt, M. H. & Dikic, I. The Cbl interactome and its functions. *Nature Rev. Mol. Cell Biol.* 6, 907–918 (2005).
5. Thien, C. B. & Langdon, W. Y. Cbl: many adaptations to regulate protein tyrosine kinases. *Nature Rev. Mol. Cell Biol.* 2, 294–307 (2001).
6. Thien, C. B. & Langdon, W. Y. c-Cbl and Cbl-b ubiquitin ligases: substrate diversity and the negative regulation of signalling responses. *Biochem. J.* 391, 153–166 (2005).
7. Corey, S. J. *et al.* Myelodysplastic syndromes: the complexity of stem-cell diseases. *Nature Rev. Cancer* 7, 118–129 (2007).
8. Jaffe, E., Harris, N., Stein, H. & Vardiman J. *World Health Organization Classification of Tumours: Pathology and Genetics of Tumours of Haematopoietic and Lymphoid Tissues* 62–73 (IARC Press, 2002).
9. Nannya, Y. *et al.* A robust algorithm for copy number detection using high-density oligonucleotide single nucleotide polymorphism genotyping arrays. *Cancer Res.* 65, 6071–6079 (2005).
10. Yamamoto, G. *et al.* Highly sensitive method for genomewide detection of allelic composition in nonpaired, primary tumor specimens by use of affymetrix single-nucleotide-polymorphism genotyping microarrays. *Am. J. Hum. Genet.* 81, 114–126 (2007).
11. Haase, D. Cytogenetic features in myelodysplastic syndromes. *Ann. Hematol.* 87, 515–526 (2008).
12. Langdon, W. Y. *et al.* v-cbl, an oncogene from a dual-recombinant murine retrovirus that induces early B-lineage lymphomas. *Proc. Natl Acad. Sci. USA* 86, 1168–1172 (1989).
13. Abbas, S. *et al.* Exon 8 splice site mutations in the gene encoding the E3-ligase CBL are associated with core binding factor acute myeloid leukemias. *Haematologica* 93, 1595–1597 (2008).
14. Caligiuri, M. A. *et al.* Novel c-CBL and CBL-b ubiquitin ligase mutations in human acute myeloid leukemia. *Blood* 110, 1022–1024 (2007).
15. Sargin, B. *et al.* Flt3-dependent transformation by inactivating c-Cbl mutations in AML. *Blood* 110, 1004–1012 (2007).
16. Dunbar, A. J. *et al.* 250K single nucleotide polymorphism array karyotyping identifies acquired uniparental disomy and homozygous mutations, including novel missense substitutions of c-Cbl, in myeloid malignancies. *Cancer Res.* 68, 10349–10357 (2008).
17. Zheng, N. *et al.* Structure of a c-Cbl-UbcH7 complex: RING domain function in ubiquitin-protein ligases. *Cell* 102, 533–539 (2000).
18. Murphy, M. A. *et al.* Tissue hyperplasia and enhanced T-cell signalling via ZAP-70 in c-Cbl-deficient mice. *Mol. Cell. Biol.* 18, 4872–4882 (1998).
19. Naramura, M. *et al.* Altered thymic positive selection and intracellular signals in Cbl-deficient mice. *Proc. Natl Acad. Sci. USA* 95, 15547–15552 (1998).
20. Rathinam, C. *et al.* The E3 ubiquitin ligase c-Cbl restricts development and functions of hematopoietic stem cells. *Genes Dev.* 22, 992–997 (2008).
21. Honda, H. *et al.* Acquired loss of p53 induces blastic transformation in p210(bcr/abl)-expressing hematopoietic cells: a transgenic study for blast crisis of human CML. *Blood* 95, 1144–1150 (2000).
22. Zeng, S. *et al.* Regulation of stem cell factor receptor signaling by Cbl family proteins (Cbl-b/c-Cbl). *Blood* 105, 226–232 (2005).
23. Kaushansky, K. Hematopoietic growth factors, signaling and the chronic myeloproliferative disorders. *Cytokine Growth Factor Rev.* 17, 423–430 (2006).
24. Naramura, M. *et al.* c-Cbl and Cbl-b regulate T cell responsiveness by promoting ligand-induced TCR down-modulation. *Nature Immunol.* 3, 1192–1199 (2002).
25. Dittmer, D. *et al.* Gain of function mutations in p53. *Nature Genet.* 4, 42–46 (1993).
26. Lang, G. A. *et al.* Gain of function of a p53 hot spot mutation in a mouse model of Li-Fraumeni syndrome. *Cell* 119, 861–872 (2004).
27. Finlay, C. A., Hinds, P. W. & Levine, A. J. The p53 proto-oncogene can act as a suppressor of transformation. *Cell* 57, 1083–1093 (1989).
28. Chen, Y. *et al.* Oncogenic mutations of ALK kinase in neuroblastoma. *Nature* 455, 971–974 (2008).

Supplementary Information is linked to the online version of the paper at www.nature.com/nature.

Acknowledgements This work was supported by the Core Research for Evolutional Science and Technology, Japan Science and Technology Agency, a Grant-in-Aid from the Ministry of Health, Labor and Welfare of Japan and from the Ministry of Education, Culture, Sports, Science and Technology, and a grant from National Health Research Institute, Taiwan, NHRI-EX96-9434SI, and NIH-2R01CA026038-30. We thank W. Y. Langdon for providing a human *C-CBL* cDNA. A mast-cell cell line expressing c-KIT V3MC was a gift from M. F. Gurish. We also thank Y. Ogino and K. Fujita for their technical assistance.

Author Contributions M.S. and M.Kato performed microarray experiments and subsequent data analyses. T.S., T.Y., H.Honda and H.Hirai generated and analysed *c-Cbl*-null mice. M.S., M.Otsu, S.Y., M.N., K.K., N.G., M.Onodera, M.S.-Y. and H.N. conducted functional assays of C-CBL mutants. L.-Y.S., M.S., M.Kato, K.N., J.T. and A.T. performed mutation analysis. H.O. performed pathological analysis of *c-Cbl*-null mice. L.-Y.S., N.K., H.Harada, M.Kurokawa, S.C., H.M., H.P.K. and M.Omine prepared MDS specimens. M.S., M.Otsu, Y.H., K.O., H.M., H.N., L.-Y.S., H.P.K. and S.O. designed the overall study, and S.O. wrote the manuscript. All authors discussed the results and commented on the manuscript.

Author Information Full copy number data for the 222 samples are accessible from the Gene Expression Omnibus public database (http://ncbi.nlm.nih.gov/geo/) with the accession number GSE15187. Reprints and permissions information is available at www.nature.com/reprints. Correspondence and requests for materials should be addressed to S.O. (sogawa-tky@umin.ac.jp) or L.-Y.S. (sly7012@adm.cgmh.org.tw).

METHODS

Genome-wide analysis of allelic imbalances in primary myeloid neoplasms. Bone marrow specimens were obtained from 222 patients diagnosed with myeloid neoplasms according to the WHO classification (Supplementary Tables 1 and 2). High molecular weight genomic DNA was extracted and used for microarray analysis using Affymetrix GeneChip 50K XbaI, HindIII or 250K NspI, according to the manufacturer's instructions. Genome-wide detection of allelic imbalances was performed using CNAG/AsCNAR software (http://www.genome.umin.jp)[9,10].

Mutation analysis. Mutation analysis was performed by direct sequencing of PCR-amplified coding exons of the relevant genes, using an ABI PRISM 3100 genetic analyser (Applied Biosystems). The target genes, exons and PCR primers are listed in Supplementary Table 8. Tandem duplication of the *FLT3* gene was examined by genomic PCR and sequencing.

Preparation of high-titre vesicular stomatitis virus glycoprotein (VSV-G)-pseudotyped retroviral particles. HA-tagged human *C-CBL* cDNA was a gift from W. Y. Langdon. Nine mutant cDNAs of *C-CBL*, including eight from patients' specimens and a 70Z mutant corresponding to a mutant isolated from mouse lymphoma[29], were generated on the basis of this construct, using a QuickChange site-directed mutagenesis kit (Stratagene). These were then constructed into the retrovirus vectors pGCDNsamIRESGFP and pGCDNsamIRESKO[30–32]. Vector plasmids were co-transfected with a VSV-G cDNA into 293GP cells (provided by R. C. Mulligan) to obtain retrovirus-containing supernatant, which was then transduced into 293GPG cells to establish stable cell lines capable of producing VSV-G-pseudotyped retroviral particles on induction[33,34]. The average titre of retrovirus stocks prepared from these cell lines routinely exceeded approximately $1–10 \times 10^7$ inclusion-forming units per ml, as estimated using Jurkat cells.

Assays for anchorage-independent growth and tumorigenicity in nude mice. NIH3T3 cells (the Japan Cell Resource Bank) were stably transduced with wild-type and mutant *C-CBL* by retrovirus-mediated gene transfer. For colony formation assays, 1.0×10^3 stable cells for each construct were inoculated in 0.33% top agar, and the numbers of colonies >1 mm in diameter were counted 3 weeks after inoculation ($n = 8$). Experiments were repeated four times. For tumour formation in nude mice, 1.0×10^7 stable cells were inoculated subcutaneously at two sites per mouse. Cells were inoculated at six sites in three mice for each construct.

Purification of LSK HSPCs. LSK HSPCs were purified from bone marrow and spleen as described[35,36]. Multicolour flow cytometry analysis and cell sorting were performed using a MoFlo cell Sorter (Beckman Coulter). The purity of sorted cell fractions consistently exceeded 98%.

Replating assays of bone marrow progenitor cells. Bone marrow LSK cells were infected with IRES/GFP-containing retrovirus carrying mock, wild-type C-CBL and three C-CBL mutants (C-CBL(Gln367Pro), C-CBL(Tyr371Ser) and C-CBL(Cys384Gly)) as well as C-CBL(70Z) on RetroNectin-coated dishes. After 48 h infection in culture in StemSpan supplemented with SCF (50 ng ml^{-1}; Peprotech), TPO (20 ng ml^{-1}) and FLT3LG (20 ng ml^{-1}), 1.0×10^2 GFP-positive cells were inoculated in MethoCult M3231 supplemented with TPO (20 ng ml^{-1}), IL3 (10 ng ml^{-1}), IL6 (10 ng ml^{-1}), FLT3LG (10 ng ml^{-1}) and SCF (50 ng ml^{-1}) for colony formation. Colony-forming cells were collected 7 days after each inoculation, from which 1.0×10^3 cells were repeatedly subjected to replating until no colonies were produced. Experiments were repeated at the indicated times for each C-CBL construct.

Generation of *c-Cbl*$^{-/-}$ mice and evaluation of their tumour-prone phenotype. *c-Cbl*$^{-/-}$ mice were generated using a conventional method of gene targeting (Supplementary Fig. 10). *c-Cbl*$^{+/+}$, *c-Cbl*$^{+/-}$ and *c-Cbl*$^{-/-}$ mice were crossed with *BCR-ABL* transgenic mice, and their survival and the development of blastic crises were monitored.

Evaluation of haematopoietic pool size in *c-Cbl*$^{-/-}$ mice. LSK and CD34$^-$ LSK cells were sorted from bone marrow cells or spleens of *c-Cbl*$^{-/-}$ mice, and their numbers were compared to those in *c-Cbl*$^{+/+}$ littermates (8 week old). Approximately 5×10^3 bone marrow cells collected from *c-Cbl*$^{+/+}$ and *c-Cbl*$^{-/-}$ mice were inoculated into MethoCult M3231 culture supplemented with TPO (20 ng ml^{-1}), IL3 (10 ng ml^{-1}), IL6 (10 ng ml^{-1}), EPO (3 U ml^{-1}) and SCF (50 ng ml^{-1}). The number of colonies was counted 7 days after culturing.

***In vitro* cell proliferation assays.** Approximately 6×10^3 LSK cells from *c-Cbl*$^{-/-}$ mice and their *c-Cbl*$^{+/+}$ littermates (8 week old) were sorted into RetroNectin-coated 96-well U-bottom plates containing α-minimum essential medium supplemented with 1% fetal bovine serum (FBS), mouse SCF (50 ng ml^{-1}), and human TPO (100 ng ml^{-1}). After 24 h pre-incubation, retrovirus supernatant was added to each well at a multiplicity of infection of about 10. The plates were incubated for another 24 h in the presence of protamine sulphate (10 μg ml^{-1}), followed by repeated infection and extended culture for 2 days in S-Clone SF-O3 medium (Sanko Junyaku) supplemented with 1% BSA, 50 ng ml^{-1} SCF and 50 ng ml^{-1} TPO. On day 4, fluorescent-marker-positive cells were sorted for subsequent analyses. Cell survival and proliferation of LSK cells transduced with different *C-CBL* constructs were assessed in serum-free liquid culture in 96-well U-bottom plates in the presence of various cytokines. Each well received 50 fluorescent-marker-positive LSK cells, and the cells were cultured in S-Clone supplemented with 1% BSA plus SCF, TPO, IL3 or FLT3LG at the indicated concentrations. Cell numbers were counted either by analysing well images or by flow cytometry using FlowCount beads (Beckman Coulter). After 6 h serum starvation, 1×10^4 LSK cells transduced with various *C-CBL* constructs were stimulated with SCF (10 ng ml^{-1}) and TPO (10 ng ml^{-1}) for 15 min. Whole-cell lysates were examined for activation of STAT5 and Akt by immunoblots using the respective antibodies.

Immunoblot analysis of physical interactions between mutant C-CBL and CBL-B. Flag-tagged CBL-B or C-CBL was co-transfected into NIH3T3 cells with each of three HA-tagged C-CBL mutants (C-CBL(Gln367Pro), C-CBL(Tyr371Ser) and C-CBL(70Z)). Total cell lysates of these NIH3T3 cells were immunoprecipitated with anti-Flag antibody, followed by immunoblot analysis with anti-HA antibody.

Detection of ubiquitination and phosphorylation of kinases. After overnight serum starvation, NIH3T3 cells stably transduced with human EGFR, and indicated HA-tagged C-CBL mutants and Flag-tagged wild-type C-CBL were stimulated with human EGF (10 ng ml^{-1}) for 2 min. Cell lysates were immunoprecipitated with anti-EGF antibody, followed by immunoblotting using anti-ubiquitin antibody. Constructs for wild-type C-CBL and mutant C-CBL were stably transduced into a mast cell line, V3MC, FLT3-transduced 32D cells (32D/FLT3) and BaF3 cells transduced with human EPOR and JAK2 (BaF3/EPOR/JAK2) using retrovirus-mediated gene transfer. After overnight serum starvation, the transduced cells were stimulated with 10 ng ml^{-1} SCF (V3MC), 10 U ml^{-1} EPO (BaF3/EPOR/JAK2) or 10 ng ml^{-1} FLT3LG (32D/FLT3) for 1 min. The specific kinases were immunoprecipitated with relevant antibodies, and their ubiquitination was detected by immunoblotting with anti-ubiquitin antibody. Tyrosine phosphorylation of EGFR, c-KIT, JAK2 and FLT3 was examined by immunoblot analyses of total cell lysates after cytokine stimulation at indicated time points, using antibodies specifically recognizing phosphorylated kinases, anti-p-EGFR, anti-p-c-KIT, anti-p-JAK2 and anti-p-FLT3, respectively. Anti-GAPDH or anti-α-tubulin immunoblot was performed as a control. Antibodies used in this study are listed in Supplementary Table 9.

Statistical analysis. Statistical significance of prolonged replating capacity of mutant *C-CBL*-transduced LSK cells was tested by counting the total number of dishes that produced colonies, followed by Fisher's exact test. Survival curves of *c-Cbl*$^{+/+}$, *c-Cbl*$^{+/-}$ and *c-Cbl*$^{-/-}$ mice containing the *BCR-ABL* transgene were generated using the Kaplan–Meier method. Overall survivals of *C-CBL*-mutated and non-mutated CMML cases were analysed according to the proportional hazard model, using STATA software. Statistical differences in survival were evaluated using the log-rank test, and statistical differences in 2×2 contingency tables were tested according to Fisher's exact method. Student's *t*-tests were used to evaluate the significance of difference in spleen mass, number of haematopoietic progenitors and colony-forming cells between *c-Cbl*$^{+/+}$ and *c-Cbl*$^{-/-}$.

29. Blake, T. J. *et al.* The sequences of the human and mouse c-cbl proto-oncogenes show v-cbl was generated by a large truncation encompassing a proline-rich domain and a leucine zipper-like motif. *Oncogene* 6, 653–657 (1991).
30. Hamanaka, S. *et al.* Stable transgene expression in mice generated from retrovirally transduced embryonic stem cells. *Mol. Ther.* 15, 560–565 (2007).
31. Nabekura, T. *et al.* Potent vaccine therapy with dendritic cells genetically modified by the gene-silencing-resistant retroviral vector GCDNsap. *Mol. Ther.* 13, 301–309 (2006).
32. Sanuki, S. *et al.* A new red fluorescent protein that allows efficient marking of murine hematopoietic stem cells. *J. Gene Med.* 10, 965–971 (2008).
33. Ory, D. S., Neugeboren, B. A. & Mulligan, R. C. A stable human-derived packaging cell line for production of high titer retrovirus/vesicular stomatitis virus G pseudotypes. *Proc. Natl Acad. Sci. USA* 93, 11400–11406 (1996).
34. Suzuki, A. *et al.* Feasibility of *ex vivo* gene therapy for neurological disorders using the new retroviral vector GCDNsap packaged in the vesicular stomatitis virus G protein. *J. Neurochem.* 82, 953–960 (2002).
35. Ema, H. *et al.* Adult mouse hematopoietic stem cells: purification and single-cell assays *Nature Protoc.* 1, 2979–2987 (2006).
36. Osawa, M. *et al.* Long-term lymphohematopoietic reconstitution by a single CD34-low/negative hematopoietic stem cell. *Science* 273, 242–245 (1996).

nature medicine

$CD8^+$ effector T cells contribute to macrophage recruitment and adipose tissue inflammation in obesity

Satoshi Nishimura[1–4], Ichiro Manabe[1,2,4,5], Mika Nagasaki[1,6], Koji Eto[7], Hiroshi Yamashita[1], Mitsuru Ohsugi[8], Makoto Otsu[7], Kazuo Hara[8], Kohjiro Ueki[3,5,8], Seiryo Sugiura[9], Kotaro Yoshimura[10], Takashi Kadowaki[3,5,8] & Ryozo Nagai[1,3,5]

Inflammation is increasingly regarded as a key process underlying metabolic diseases in obese individuals. In particular, obese adipose tissue shows features characteristic of active local inflammation. At present, however, little is known about the sequence of events that comprises the inflammatory cascade or the mechanism by which inflammation develops. We found that large numbers of $CD8^+$ effector T cells infiltrated obese epididymal adipose tissue in mice fed a high-fat diet, whereas the numbers of $CD4^+$ helper and regulatory T cells were diminished. The infiltration by $CD8^+$ T cells preceded the accumulation of macrophages, and immunological and genetic depletion of $CD8^+$ T cells lowered macrophage infiltration and adipose tissue inflammation and ameliorated systemic insulin resistance. Conversely, adoptive transfer of $CD8^+$ T cells to CD8-deficient mice aggravated adipose inflammation. Coculture and other *in vitro* experiments revealed a vicious cycle of interactions between $CD8^+$ T cells, macrophages and adipose tissue. Our findings suggest that obese adipose tissue activates $CD8^+$ T cells, which, in turn, promote the recruitment and activation of macrophages in this tissue. These results support the notion that $CD8^+$ T cells have an essential role in the initiation and propagation of adipose inflammation.

Inflammation is now considered to have a pivotal role in the development of metabolic diseases[1]. In particular, obese adipose tissue shows the hallmarks of chronic inflammation[2,3], and the inflammation is thought to alter adipose tissue function, leading to systemic insulin resistance[4]. The mechanism by which the development of this insulin resistance occurs is believed to involve proinflammatory cytokines produced by infiltrating macrophages and resident adipocytes within the obese adipose tissue[1]. Likewise, chronic inflammation also impairs triglyceride storage in adipose tissues, and the excess circulating free fatty acids and triglycerides also induces insulin resistance in muscle and liver[5–7]. Adding insult to injury, it has been postulated that a paracrine loop involving these free fatty acids and inflammatory cytokines establishes a vicious cycle that aggravates the inflammatory changes, furthering the dysfunction of adipose tissue[8]. As such, the inflammatory changes seen in obese adipose tissue may be the key pathology that promotes systemic inflammatory states and insulin resistance in obese individuals.

Macrophage infiltration of adipose tissue has been described in both mice and humans[1]. However, little is known about the sequence of events that lead to macrophage infiltration. Recently accumulation of other immune cells, such as T cells, has been documented in obese adipose tissue[9,10]. T lymphocytes are known to interact with macrophages and regulate the inflammatory cascade[11]. However, their functional role in adipose inflammation remains unclear. Here we show that infiltration of $CD8^+$ effector T cells is an early event during the development of adipose tissue obesity induced by a high-fat diet. Further, we show using loss- and gain-of-function approaches *in vivo* that these T cells are critical mediators of systemic metabolic dysfunction. Finally, we also show *in vitro* that obese adipose tissue can activate $CD8^+$ T cells, which, in turn, allows for the recruitment and differentiation of macrophages. Thus, together our findings indicate that $CD8^+$ T cells have essential roles in the initiation and maintenance of adipose tissue inflammation and systemic insulin resistance. Our results also clearly show the involvement of adaptive immunity in metabolic disorders.

RESULTS

$CD8^+$ T cell infiltration precedes macrophage accumulation

Adipose tissue consists of not only adipocytes but also stromal and vascular cells, including fibroblasts, vascular endothelial cells and inflammatory cells. This stromal vascular fraction is known to be essential for adipose tissue inflammation[2]. Therefore, to gain insight

[1]Department of Cardiovascular Medicine, [2]Nano-Bioengineering Education Program and [3]Translational Systems Biology and Medicine Initiative, Graduate School of Medicine, The University of Tokyo, Tokyo, Japan. [4]PRESTO, Japan Science and Technology Agency, Kawaguchi, Japan. [5]Comprehensive Center of Education and Research for Chemical Biology of the Diseases, [6]Computational Diagnostic Radiology and Preventive Medicine, The University of Tokyo, Tokyo, Japan. [7]Division of Stem Cell Therapy, Center for Stem Cell Biology and Regenerative Medicine, Institute of Medical Science, The University of Tokyo, Tokyo, Japan. [8]Department of Metabolic Diseases, Graduate School of Medicine, The University of Tokyo, Tokyo, Japan. [9]Department of Human and Engineered Environmental Studies, Graduate School of Frontier Sciences, The University of Tokyo, Tokyo, Japan. [10]Department of Plastic Surgery, Graduate School of Medicine, The University of Tokyo, Tokyo, Japan. Correspondence should be addressed to S.N. (snishi-tky@umin.ac.jp) or I.M. (manabe-tky@umin.ac.jp).

Received 5 January; accepted 7 April; published online 26 July 2009; doi:10.1038/nm.1964

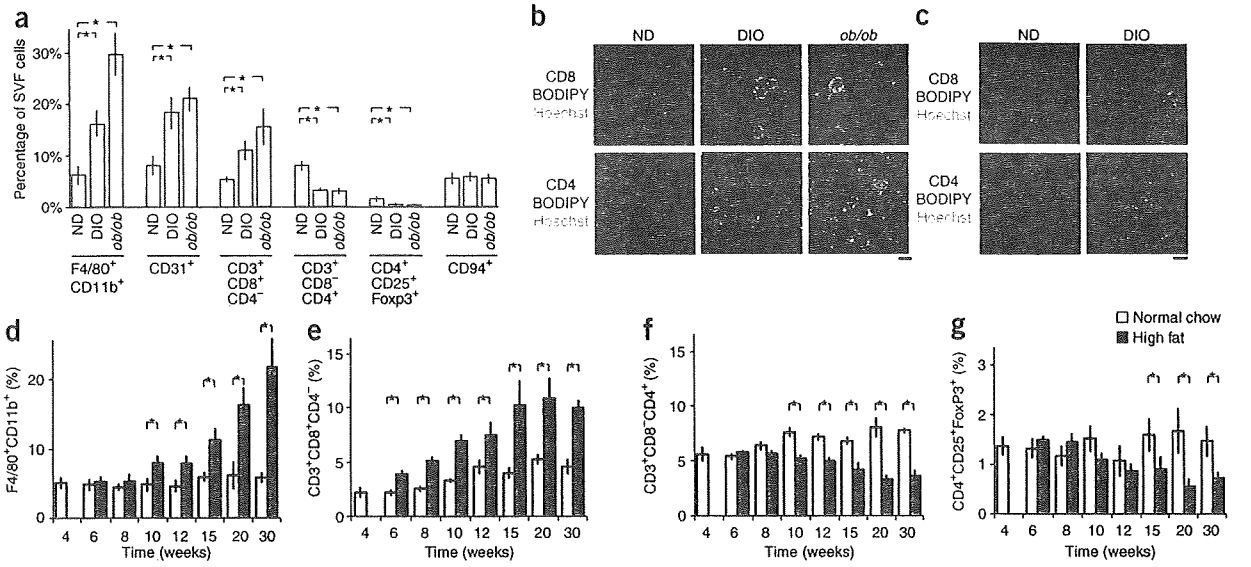

Figure 1 Differential infiltration of lymphocytes and macrophages into obese adipose tissue. (**a**) Flow cytometric analysis of the stromal vascular fraction (SVF) from the epididymal fat pads of control mice fed a normal chow diet (ND), diet-induced obese (DIO) mice fed a high-fat diet for 16 weeks and *ob/ob* mice fed a normal diet (*ob/ob*). All mice were 20-weeks-old. The cell populations of macrophages ($F4/80^+CD11b^+$), endothelial cells ($CD31^+$), $CD3^+CD8^+CD4^-$ T cells, $CD3^+CD8^-CD4^+$ T cells, regulatory T cells ($CD4^+CD25^+Foxp3^+$) and NK cells ($CD3^-CD94^+$) were analyzed ($n = 5$ mice in each group). The number of each cell type was normalized to the total number of viable SVF cells. $^*P < 0.05$. (**b**,**c**) Immunohistochemical analysis of CD8 and CD4 (each in red) in epididymal (**b**) and femoral subcutaneous (**c**) adipose tissue from ND, DIO and *ob/ob* mice. Adipocytes were counterstained with boron-dipyrromethene (BODIPY, blue) and nuclei with Hoechst (green). Quantification of $CD8^+$ and $CD4^+$ cells is shown in **Supplementary Fig. 3**. Scale bars, 100 μm. (**d**–**g**) Time courses of changes in the cell populations in the adipose stroma during development of obesity. Flow cytometric analysis of the stromal vascular fraction from the epididymal fat pads of control mice fed a normal chow diet and mice fed a high-fat diet beginning when they were 4-weeks-old. Numbers of macrophages (**d**), $CD8^+$ T cells (**e**), $CD4^+$ T cells (**f**) and regulatory T cells (**g**) were determined during the course of DIO development ($n = 5$ mice in each group; $^*P < 0.05$). Error bars represent means ± s.e.m.

into the inflammatory processes taking place within these cell fractions during obesity, we first analyzed immune cell populations in collagenase-digested stromal vascular fractions from obese epididymal adipose tissue with the aim of identifying local obesity-induced immunological changes. We acquired stromal vascular fractions using previously described methods of isolation[12] with a few modifications. We first carried out a set of flow cytometric analyses to determine the proper gating for analysis of lymphocytes and macrophages in adipose tissue (**Supplementary Fig. 1**). We found that R1 gating accounted for the majority of viable cells, including a majority of $F4/80^+CD11b^+$ macrophages. Because earlier studies used broader gating to analyze macrophages in the stromal vascular fraction[13], we compared the broader R2 gating with the narrower R1 gating. We found that the macrophage and lymphocyte fractions detected with R1 gating did not significantly differ from those detected using the broader R2 gating (**Supplementary Fig. 1** and **Supplementary Table 1**). For that reason, we analyzed subsequent cell fractions by R1 gating (for further discussion of gating, see **Supplementary Methods** and **Supplementary Fig. 1**).

Consistent with earlier reports[2], the infiltration of $F4/80^+CD11b^+$ macrophages into adipose tissue was significantly increased by diet-induced obesity (DIO) and in obese *ob/ob* mice compared to the control lean mice on a normal diet ($P < 0.05$) (**Fig. 1a**). The numbers of $CD31^+$ endothelial cells were also higher in obese mice (**Fig. 1a**), which may reflect angiogenesis[14]. Notably, we found that $CD3^+$ T cells accounted for 14.8 ± 0.9% of stromal vascular cells in lean adipose tissue, and most (94.7 ± 0.3%) of the $CD3^+$ T cells were CD4 or CD8 positive. The $CD3^+CD8^+CD4^-$ T cell fraction was larger in obese adipose tissue, whereas the $CD3^+CD4^+CD8^-$ T cell fraction was smaller, as was the regulatory T cell fraction ($CD4^+CD25^+Foxp3^+$) compared to lean mice on normal diet ($P < 0.05$). The natural killer (NK) cell fraction ($CD3^-CD94^+$) was unaffected by obesity (**Fig. 1a**). In contrast to the higher number of $CD8^+$ lymphocytes seen in obese adipose tissue, $CD8^+$ and $CD4^+$ T cell counts were significantly lower in peripheral blood from *ob/ob* mice and were unchanged in DIO mice as compared to mice on a normal diet ($P < 0.05$) (**Supplementary Fig. 2**), suggesting selective recruitment of $CD8^+$ T lymphocytes to obese adipose tissues.

Immunohistochemical analysis of F4/80, CD8 and CD4 expression also revealed higher numbers of $F4/80^+$ macrophages and $CD8^+$ T cells and lower numbers of $CD4^+$ T cells in obese epididymal fat pads as compared to mice on a normal diet ($P < 0.05$) (**Fig. 1b** and **Supplementary Fig. 3**). By contrast, we found no significant changes in the numbers of $CD8^+$ and $CD4^+$ cells in subcutaneous fat pads (**Fig. 1c**). In obese epididymal adipose tissues, we found a number of $CD8^+$ cells within 'crown-like structures' (CLSs), which reflect the focal convergence of macrophages surrounding necrotic adipocytes[14,15] (**Fig. 1b**), whereas $CD4^+$ cells showed no apparent relationship with CLSs.

Most $CD3^+CD8^+$ cells were $CD62L^-$ and $CD44^+$ (74.7% ± 3.8% of $CD3^+$ $CD8^+$ cells in DIO mice), suggesting the majority of infiltrated $CD8^+$ T cells were activated effector T cells[16]. To assess the clonality of $CD8^+$ in obese adipose, we examined the T cell receptor (TCR) V_β repertoire of $CD8^+$ T cells in lean and obese adipose tissues. The results showed that $CD8^+$ T cells in obese adipose were not monoclonal, though the $CD8^+$ cell fractions that were positive for $V_{\beta 7}$ and $V_{\beta 20b}$ were significantly larger in obese adipose tissues as compared to mice on a normal diet ($P < 0.05$) (**Supplementary Fig. 4**).

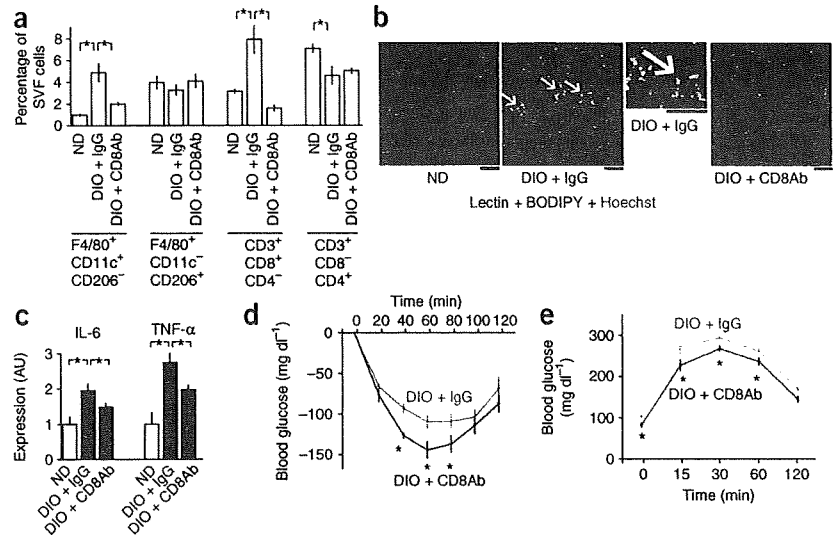

Figure 2 Effects of CD8-specific antibody treatment on obese adipose tissue inflammation. (**a**) Flow cytometric analysis of M1 macrophages ($F4/80^+CD11c^+CD206^-$), M2 macrophages ($F4/80^+CD11c^-CD206^+$), $CD8^+$ T cells and $CD4^+$ T cells in stromal vascular fractions in mice from lean normal-diet (ND), and DIO mice administered either antibody to CD8 (DIO + CD8Ab) or control IgG (DIO + IgG). The same mice were used in **b–e**. High-fat diet was started at the age of 4-weeks-old, and all of the mice were examined at 12-weeks-old. ($n = 5$ mice in each group). (**b**) Histochemical identification of endothelial cells (lectin, red), adipocytes (BODIPY, blue) and nuclei (Hoechst, green) in epididymal adipose tissue. White arrows indicate CLSs. Scale bars, 100 μm. (**c**) Real-time PCR analysis of cytokine expression in adipose tissue. The levels of each transcript were normalized to that in the lean control ($n = 5$ mice in each group). AU, arbitrary units. (**d,e**) Results of insulin tolerance (**d**, 0.75 U insulin per kg body weight) and oral glucose tolerance (**e**, 1 g per kg glucose) tests in DIO mice treated with antibody to CD8 or control IgG ($n = 8$ mice in each group). $^*P < 0.05$. Error bars represent means ± s.e.m.

It is known that one consequence of macrophage accumulation, particularly M1 macrophages, in inflamed adipose tissue is modulation and impairment of the tissue's function[17]. It is not known, however, what initiates macrophage infiltration or the resultant inflammatory cascade. The dynamic changes in lymphocyte populations seen in obese adipose tissue (**Fig. 1a,b**) suggest that lymphocytes might have a key role. To test this idea, we examined the time course of changes in stromal cell populations during the progression of DIO. We fed C57BL/6 mice a high-fat diet, beginning when they were 4-weeks-old (**Fig. 1d–g**). Within 2 weeks, the $CD8^+CD4^-$ T cell fraction within the total stromal vascular cell fraction was significantly increased in the stroma of the epididymal fat, as compared to that in mice fed a control chow diet (**Fig. 1e**). The numbers of $CD8^+CD4^-$ T cells continued to increase thereafter, peaking when the mice were 15-weeks-old (**Fig. 1e**). By contrast, the fractions of $CD8^-CD4^+$ T cells and $CD4^+CD25^+FoxP3^+$ regulatory T cells were reduced at later times (**Fig. 1f,g**), suggesting that $CD8^+$ T cell infiltration is a primary event during inflammatory cascades within adipose tissue. The increase in $CD8^+$ T cells also preceded the accumulation of macrophages when cell numbers were expressed per fat pad (**Supplementary Fig. 5**), clearly indicating that $CD8^+$ cells infiltrated into the epididymal fat pads of DIO mice before macrophage infiltration.

To gain additional insight into the clinical importance of $CD8^+$ T cells in obese fat, we analyzed the expression of *CD8A* in samples of human subcutaneous adipose tissue. Levels of *CD8A* expression were significantly higher in obese subjects than in lean ones ($P < 0.05$), suggesting that $CD8^+$ T cells also accumulate in human obese adipose tissue (**Supplementary Fig. 6**).

CD8 depletion inhibits inflammatory cascade in obese adipose

To assess the role of $CD8^+$ T cells in adipose inflammation, we examined the effects of CD8 depletion using neutralizing antibody treatment on the inflammatory response in obese adipose tissue. We randomly assigned male C57BL/6 mice to two groups and intraperitoneally administered either antibody to CD8 or control IgG once a week for 8 weeks, beginning when the mice were 4-weeks-old. We fed the mice a high-fat diet over the same period, and we performed metabolic and histological analyses at 12 weeks of age. Antibody to CD8 treatment had no effect on body weight, food intake, fat pad weight or adipocyte diameter (**Supplementary Fig. 7**). However, it significantly lowered the $CD8^+CD4^-$ T cell fraction in the epididymal fat pads without affecting the $CD8^-CD4^+$ cell fraction (**Fig. 2a**). It also reduced the infiltrated M1 macrophage ($F4/80^+CD11c^+CD206^-$) fraction without affecting the M2 macrophage ($F4/80^+CD11c^-CD206^+$) fraction[17] and significantly lowered the numbers of CLSs ($P < 0.05$ for each) (**Fig. 2b** and **Supplementary Fig. 7d**).

The messenger RNA expression of the proinflammatory cytokines interleukin-6 (IL-6) and tumor necrosis factor-α (TNF-α) in epididymal fat pads was lowered by CD8-specific antibody treatment (**Fig. 2c**), as were their serum concentrations (**Supplementary Fig. 7f**). In addition, the insulin resistance and glucose intolerance induced by the high-fat diet were ameliorated by CD8-specific antibody treatment (**Fig. 2d,e**). Similarly, CD8-specific antibody treatment lowered M1 macrophage infiltration into epididymal fat and ameliorated systemic insulin resistance in *ob/ob* mice (**Supplementary Fig. 8**). Collectively, these effects of CD8-specific antibody treatment clearly show that $CD8^+$ cells are required for the recruitment of macrophages into obese adipose tissue and the initiation and propagation of inflammatory responses there.

CD8 depletion ameliorates pre-established inflammation

We next examined the activity of $CD8^+$ T cells in obese adipose tissues in which inflammation had already been established. We began administering antibodies to 19-week-old DIO mice that had been fed a high-fat diet since they were 9-weeks-old. We intraperitoneally administered either antibody to CD8 or control IgG three times per week for 2 weeks, and examined the mice at 21-weeks-old. Treatment with antibody to CD8 suppressed $CD8^+$ T cell infiltration into obese fat pads without affecting $CD4^+$ T cells (**Fig. 3a**). CD8 antibody also lowered M1 ($F4/80^+CD11c^+$) macrophage fraction while leaving the M2 macrophage ($F4/80^+CD11c^-$) fraction unchanged (**Fig. 3a**). The reduction in macrophage infiltration was confirmed by F4/80 immunohistochemistry (**Fig. 3b**). In addition, the number of CLSs was also lowered by CD8-specific antibody treatment (**Fig. 3b,c**). DIO led to upregulated mRNA expression of the proinflammatory cytokines IL-1, IL-6 and TNF-α, as well as of

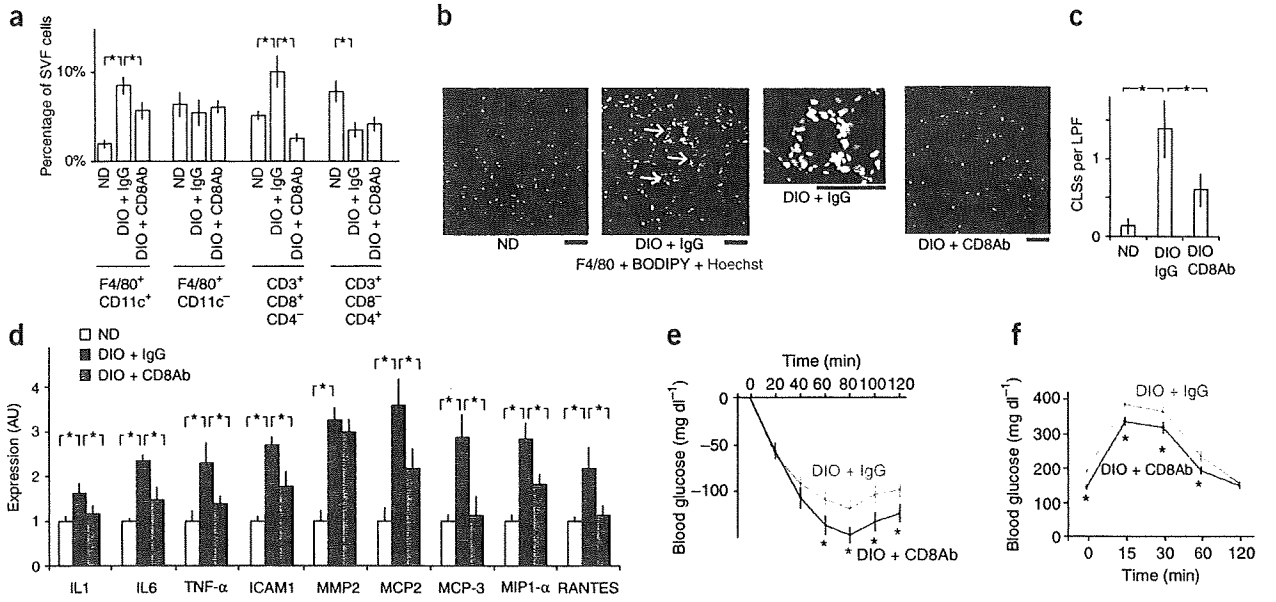

Figure 3 Effects of CD8-specific antibody treatment on pre-established obese adipose inflammation. (**a**) Flow cytometric analysis of cell populations in stromal vascular fractions from control mice on a normal chow diet (ND) and DIO mice administered control IgG (DIO + IgG) or antibody to CD8 (DIO + CD8Ab) three times per week from 19- to 21-weeks-old. ($n = 5$ mice in each group). High-fat diet was started at the age of 9-weeks-old, and all the mice were examined at 21-weeks-old. The same mice were used in **b–f**. (**b**) Immunohistochemical identification of macrophages (F4/80, red) in epididymal adipose tissue. Adipocytes were counterstained with BODIPY (blue), and the nuclei with Hoechst (green). Scale bars, 100 μm. (**c**) Numbers of CLSs (shown by white arrows in **b**) in adipose tissue ($n = 20$ low-power fields (LPF) in each group). (**d**) Real-time PCR analysis of cytokine expression in epididymal adipose tissue. The levels of each transcript were normalized to those in control ND mice. MIP, monocyte inflammatory protein ($n = 5$ mice in each group). (**e,f**) Results of insulin tolerance (**e**, 1 U insulin per kg body weight) and oral glucose tolerance (**f**, 1 g per kg glucose) tests in DIO mice treated with antibody to CD8 or control IgG ($n = 10$ mice in each group). $^*P < 0.05$. Error bars represent means ± s.e.m.

intercellular adhesion molecule-1 (ICAM1) and matrix metalloproteinase-2 (MMP-2), in adipose tissue, which is consistent with local inflammation, and CD8-specific antibody treatment lowered expression of all of these mediators (**Fig. 3d**).

CD8-specific antibody treatment also ameliorated insulin resistance and glucose intolerance in DIO mice (**Fig. 3e,f** and **Supplementary Fig. 9**). These results clearly show that CD8-specific antibody treatment suppresses preexisting adipose inflammation, which strongly suggests that $CD8^+$ cells are required for the maintenance of inflammatory reactions in obese adipose tissue.

$CD8^+$ T cells are required for adipose tissue inflammation

To further establish the requirement for $CD8^+$ T cells in adipose inflammation *in vivo*, we started 6-week-old genetically CD8-deficient mice on a high-fat diet and maintained them on it for 8 weeks, and examined the $CD8a^{-/-}$ mice at 14-weeks-old. In sharp contrast to wild-type mice fed the same high-fat diet (**Fig. 1**), the CD8-deficient mice did not show significant increases in the M1 or M2 macrophage fraction in the epididymal fat under high-fat diet (**Fig. 4a**), and we found very few CLSs (**Fig. 4b,c**), although both body weight and epididymal fat mass were significantly higher compared to $CD8a^{-/-}$ mice on a normal diet (**Supplementary Fig. 10a,b**). Levels of proinflammatory cytokine mRNA expression in adipose tissue, including IL-6 and TNF-α, also were not increased by the high-fat diet in CD8-deficient mice (**Fig. 4d**).

To directly examine the role of $CD8^+$ T cells in adipose tissue inflammation, we adoptively transferred splenic $CD8^+$ T cells into CD8-deficient mice. We intravenously administered either 5×10^6 splenic $CD8^+$ T cells isolated from 7-week-old C57BL/6 mice or control vehicle weekly over the same period and examined the $CD8a^{-/-}$ mice at 14-weeks-old. Adoptive transfer of $CD8^+$ T cells increased M1 macrophage infiltration (**Fig. 4a**), numbers of CLSs (**Fig. 4b,c**), and expression of IL-6 and TNF-α in epididymal fat (**Fig. 4d**), indicating initiation of adipose inflammation. A high-fat diet induced moderate glucose intolerance in untreated CD8-deficient mice, but we did not observe insulin resistance in insulin tolerance tests (**Fig. 4e,f**). Adoptive $CD8^+$ T cell transfer aggravated the glucose intolerance and induced insulin resistance (**Fig. 4e,f**). Taken together, the results that we obtained with CD8-deficient mice confirm that $CD8^+$ T cells are essential for macrophage recruitment and inflammation in adipose tissue in DIO.

Interplay between macrophages, T cells and adipocytes

We next analyzed the cellular interplay via which inflammation develops in obese adipose tissue. On the basis of the findings of the *in vivo* experiments summarized above, we hypothesized that obese adipose tissue activates $CD8^+$ T cells, which, in turn, recruit and activate macrophages. To test this hypothesis, we first cocultured splenic $CD8^+$ T cells with epididymal fat tissue prepared from lean or obese mice to determine whether obese adipose tissue can activate $CD8^+$ T cells. Whereas obese epididymal fat clearly induced T cell proliferation, lean fat did so only modestly (**Fig. 5a**), indicating that obese adipose tissue can indeed activate $CD8^+$ T cells.

To assess the involvement of $CD8^+$ T cells in monocytes and macrophage differentiation, we cocultured various combinations of peripheral blood $CD11b^{high}$ granulocyte-1 $(Gr\text{-}1)^-CD4^-CD8^-$cells (most of which were monocytes), $CD8^+$ cells prepared from either lean or obese adipose tissue, and lean epididymal adipose tissue. By

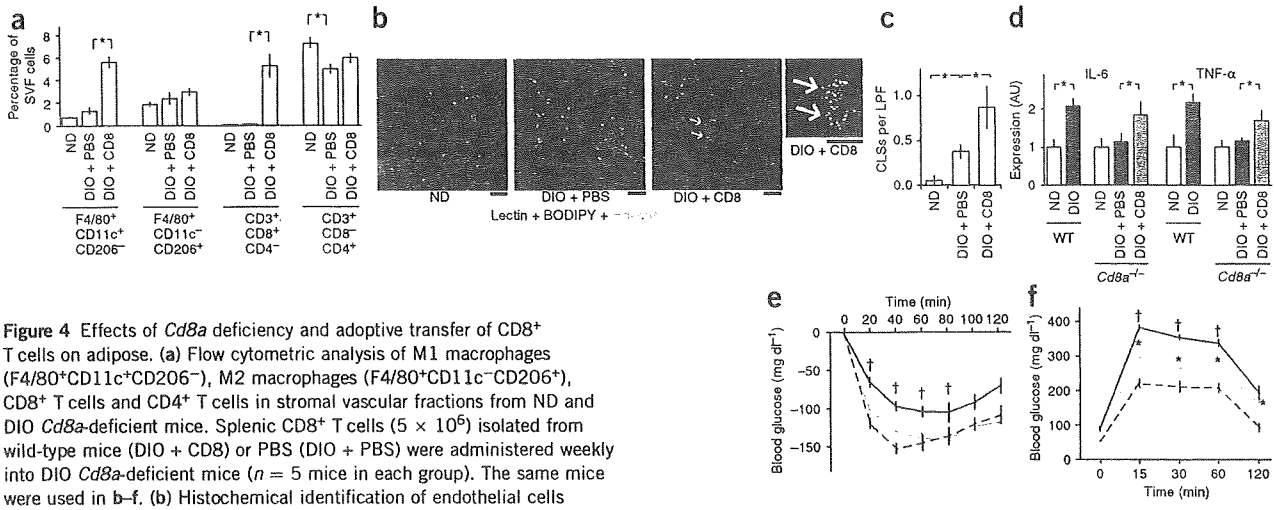

Figure 4 Effects of *Cd8a* deficiency and adoptive transfer of CD8$^+$ T cells on adipose. (**a**) Flow cytometric analysis of M1 macrophages (F4/80$^+$CD11c$^+$CD206$^-$), M2 macrophages (F4/80$^+$CD11c$^-$CD206$^+$), CD8$^+$ T cells and CD4$^+$ T cells in stromal vascular fractions from ND and DIO *Cd8a*-deficient mice. Splenic CD8$^+$ T cells (5×10^6) isolated from wild-type mice (DIO + CD8) or PBS (DIO + PBS) were administered weekly into DIO *Cd8a*-deficient mice ($n = 5$ mice in each group). The same mice were used in **b**–**f**. (**b**) Histochemical identification of endothelial cells (lectin, red), adipocytes (BODIPY, blue) and nuclei (Hoechst, green) in epididymal adipose tissue. White arrows indicate CLSs. Scale bars, 100 μm. (**c**) Numbers of CLSs in adipose tissues ($n = 20$ low-power fields in each group). (**d**) Real-time PCR analysis of cytokine expression in adipose tissue from C57BL/6 (WT) ND, WT DIO, and *Cd8a*-deficient ND, DIO + CD8 or DIO + PBS mice. ($n = 5$ mice in each group). *$P < 0.05$ in **a**–**d**. (**e**,**f**) Insulin tolerance (**e**, 0.75 U insulin per kg body weight) and oral glucose tolerance (**f**, 1 g per kg) tests of the *Cd8a*-deficient ND (dotted lines), DIO + CD8 and DIO + PBS groups ($n = 6$ mice in each group). *$P < 0.05$ for ND versus DIO + PBS and †$P < 0.05$ for DIO + PBS versus DIO + CD8. Error bars represent means ± s.e.m.

themselves, neither CD8$^+$ cells nor adipose tissue induced macrophage differentiation (**Fig. 5b**). However, when cocultured with both CD8$^+$ cells and lean adipose tissue, peripheral blood monocytes differentiated into F4/80$^+$CD11b$^+$CD68$^+$ macrophages (**Fig. 5b**). Moreover, CD8$^+$ cells from obese adipose tissues generated significantly more macrophages than those from lean adipose (**Fig. 5b**). Thus, CD8$^+$ cells seem to be essential for macrophage differentiation in this setting. Further, the requirement for adipose tissue suggests that the interaction between CD8$^+$ T cells and adipose tissue is necessary for induction of macrophage differentiation.

We then tested whether activated CD8$^+$ cells elicit macrophage migration via humoral interactions. Analysis of the medium conditioned with activated CD8$^+$ T cells showed that these cells secrete substantial amounts of humoral factors known to induce macrophage

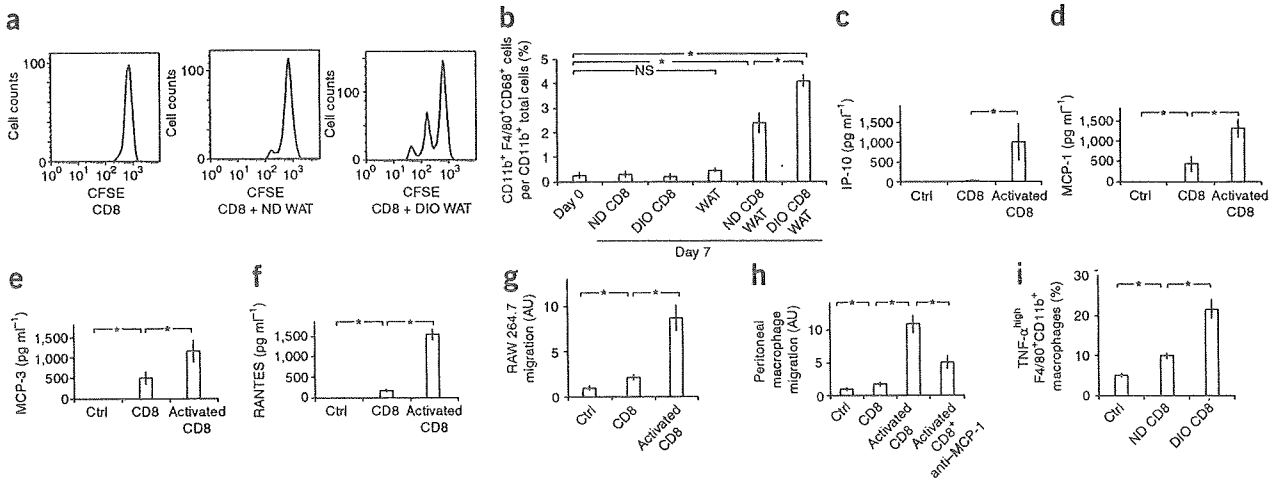

Figure 5 Interplay between macrophages, CD8$^+$ T cells and adipose tissue. (**a**) Carboxyfluorescein succinimidyl ester (CFSE) proliferation assay of isolated splenic CD8$^+$ T cells cultured with or without epididymal adipose tissue from ND or DIO mice. WAT, white adipose tissue. (**b**) Effects of CD8$^+$ T cells and adipose tissue on differentiation of peripheral blood monocytes (CD11b^{high}Gr-1$^-$) into macrophages (CD11b$^+$F4/80$^+$CD68$^+$). Monocytes were cocultured for 7 d with CD8$^+$ T cells isolated from epididymal adipose tissue from lean (ND CD8) or DIO (DIO CD8) mice, with or without epididymal WAT from lean mice. The differentiated macrophage fractions are shown ($n = 5$ in each group; *$P < 0.05$; NS, not significant). (**c**–**f**) Concentrations of various cytokines in the control medium and medium conditioned by quiescent (CD8) or activated (activated CD8) CD8 cells ($n = 5$ in each group). *$P < 0.05$. IP-10, interferon-inducible protein-10. (**g**,**h**) Migration of RAW264.7 (**g**) and peritoneal (**h**) macrophages, as examined using unconditioned control medium (Ctrl), medium conditioned by quiescent (CD8) or activated (activated CD8) CD8$^+$ T cells, or neutralizing antibody to MCP-1 (anti-MCP-1) ($n = 20$ in each group). *$P < 0.05$. (**i**) The fraction of F4/80$^+$ CD11b$^+$ macrophages producing high levels of TNF-α after isolation from lean epididymal adipose tissue and cultured without (Ctrl) or with CD8$^+$ T cells isolated from ND (ND CD8) or DIO (DIO CD8) mice ($n = 5$ in each group, *$P < 0.05$). Error bars represent means ± s.e.m.

migration, including interferon-inducible protein-10, monocyte chemoattractant protein-1 (MCP-1), MCP-3 and regulation upon activation, normal T cell expressed and secreted protein (RANTES) (**Fig. 5c–f**). When we plated cells of the macrophage cell line RAW264.7 or isolated peritoneal macrophages in Boyden chambers and treated them with medium conditioned by activated $CD8^+$ T cells, the numbers of both cell types that migrated through the pores between the chamber wells with activated $CD8^+$ T cell–conditioned medium were significantly higher compared to cells cultured in non-conditioned medium ($P < 0.05$ for each) (**Fig. 5g,h**). Treatment with antibody to MCP-1 lowered the migration of peritoneal macrophages by approximately half, indicating MCP-1 to be one of the factors mediating the humoral interactions (**Fig. 5h**).

To further assess the involvement of $CD8^+$ T cells in macrophage activation in adipose tissue, we cocultured $F4/80^+$ $CD11b^+$ macrophages isolated from lean epididymal fat tissue with $CD8^+$ cells isolated from either lean or obese fat tissue. The numbers of macrophages producing high amounts of TNF-α were significantly increased by the $CD8^+$ cells (**Fig. 5i**). Moreover, $CD8^+$ cells from obese adipose tissue increased the number of TNF-α^{high} macrophages to a significantly greater degree than those from lean adipose tissue (**Fig. 5i**). Collectively, then, the results of the coculture experiments show that the interaction between obese adipose tissue and $CD8^+$ T cells is crucial for macrophage differentiation, migration and activation.

DISCUSSION

Adipose tissue inflammation is now considered to be a crucial event leading to the metabolic syndrome, diabetes and atherosclerotic cardiovascular disease. However, it is still unclear how adipose inflammation is initiated and maintained. Here we showed that $CD8^+$ T cell infiltration precedes accumulation of macrophages in adipose tissue obesity, $CD8^+$ T cells are required for adipose tissue inflammation and $CD8^+$ T cells have major roles in macrophage differentiation, activation and migration. Thus, $CD8^+$ T cells are crucially involved in initiating inflammatory cascades in obese adipose tissue. Moreover, the finding that CD8-specific antibody treatment ameliorates preestablished adipose inflammation in DIO mice indicates that $CD8^+$ T cells are also essential for maintenance of the inflammatory response. Although infiltration of T cells into obese adipose tissue has been reported previously[10,18], to our knowledge, the present study is the first to directly address the functional role of $CD8^+$ cells in adipose tissue inflammation. The findings that systemic insulin resistance is ameliorated by CD8 depletion and aggravated by adoptive transfer of $CD8^+$ cells strongly suggest that CD8-dependent adipose inflammation has an impact on systemic metabolism.

Accumulation of $CD8^+$ T cells in obese epididymal fat pads was not accompanied by the presence of greater numbers of $CD8^+$ T cells in the systemic circulation, suggesting that $CD8^+$ T cells are activated by endogenous stimuli localized in the adipose tissue. Supporting this notion is our finding that obese adipose tissue induces $CD8^+$ T cell proliferation. The findings that incubation with $CD8^+$ T cells plus lean adipose tissue induced macrophage differentiation, although neither $CD8^+$ T cells nor lean adipose tissue did so alone, suggest that $CD8^+$ T cells and adipose tissue interact with each other to activate a local inflammatory cascade. In addition, the results of coculture experiments showing the interactions among $CD8^+$ T cells, macrophages and adipose tissue, as well as the results of our CD8 depletion experiments, which showed that $CD8^+$ T cells are essential for both the initiation and maintenance of adipose inflammation, strongly suggest that there is a relay involving both $CD8^+$ T cells and macrophages in obese adipose tissue that propagates local adipose inflammation.

In contrast to the increased infiltration of $CD8^+$ T cells, numbers of $CD4^+$ T cells and regulatory T cells were low at later time points (**Fig. 1**), which would also be expected to contribute to local inflammation within adipose tissue. For instance, subsets of $CD4^+$ T cells are known to secrete cytokines that can inhibit macrophage recruitment, including IL-4 and IL-10 (ref. 19), whereas regulatory T cells control adaptive immune responses by suppressing T cells, NK cells, NKT cells, B cells and dendritic cells[20]. In addition, regulatory T cells have also been shown to inhibit proinflammatory activation of monocytes[21] and to inhibit macrophage infiltration and renal injury in a model of chronic kidney disease[22]. It is therefore tempting to speculate that reducing the numbers of $CD4^+$ and regulatory T cells augments the inflammatory response during the late phase of adipose tissue obesity.

Taken together, our results support the idea that obese adipose tissue activates $CD8^+$ T cells, which, in turn, initiate and propagate inflammatory cascades, including the recruitment of monocytes and macrophages into obese adipose tissues and their subsequent differentiation and activation there. Thus, it seems that $CD8^+$ T cells have a primary role in obese adipose tissue inflammation, though future studies are needed to address which environmental cues within obese adipose tissue initiate $CD8^+$ cell infiltration. Even so, these results further support the idea that adipose inflammation has a major impact on systemic metabolism.

METHODS

Methods and any associated references are available in the online version of the paper at http://www.nature.com/naturemedicine/.

Note: Supplementary information is available on the Nature Medicine website.

ACKNOWLEDGMENTS

We gratefully acknowledge A. Matsuoka, X. Yingda, E. Magoshi, M. Hayashi, K. Wakabayashi, M. Tajima and Y. Yamazaki for excellent technical assistance. This study was supported by Research Fellowships from the Japan Society for the Promotion of Science for Young Scientists (S.N.), Grants-in-Aid for Scientific Research (I.M., R.N.) and grants for Translational Systems Biology and Medicine Initiative (R.N., T.K.) and Global Centers of Excellence program (R.N., T.K.) from the Ministry of Education, Culture, Sports, Science and Technology of Japan and a research grant from the National Institute of Biomedical Innovation (R.N.).

AUTHOR CONTRIBUTIONS

S.N. and M.N. performed *in vivo* and *in vitro* assays and analyzed all of the end points. K.H., K.U. and K.Y. performed human subject assays. S.N., I.M., K.E., H.Y., M. Otsu, M. Ohsugi, S.S., T.K. and R.N. supervised entire studies. S.N. and I.M. wrote the manuscript.

Published online at http://www.nature.com/naturemedicine/.
Reprints and permissions information is available online at http://npg.nature.com/reprintsandpermissions/.

1. Hotamisligil, G.S. Inflammation and metabolic disorders. *Nature* **444**, 860–867 (2006).
2. Weisberg, S.P. *et al.* Obesity is associated with macrophage accumulation in adipose tissue. *J. Clin. Invest.* **112**, 1796–1808 (2003).
3. Nishimura, S. *et al. In vivo* imaging in mice reveals local cell dynamics and inflammation in obese adipose tissue. *J. Clin. Invest.* **118**, 710–721 (2008).
4. Xu, H. *et al.* Chronic inflammation in fat plays a crucial role in the development of obesity-related insulin resistance. *J. Clin. Invest.* **112**, 1821–1830 (2003).
5. Savage, D.B., Petersen, K.F. & Shulman, G.I. Disordered lipid metabolism and the pathogenesis of insulin resistance. *Physiol. Rev.* **87**, 507–520 (2007).
6. Guilherme, A., Virbasius, J.V., Puri, V. & Czech, M.P. Adipocyte dysfunctions linking obesity to insulin resistance and type 2 diabetes. *Nat. Rev. Mol. Cell Biol.* **9**, 367–377 (2008).
7. Shoelson, S.E., Lee, J. & Goldfine, A.B. Inflammation and insulin resistance. *J. Clin. Invest.* **116**, 1793–1801 (2006).
8. Suganami, T., Nishida, J. & Ogawa, Y. A paracrine loop between adipocytes and macrophages aggravates inflammatory changes: role of free fatty acids and tumor necrosis factor alpha. *Arterioscler. Thromb. Vasc. Biol.* **25**, 2062–2068 (2005).